Helsinki University of Technology Laboratory of Computational Engineering Publications
Teknillisen korkeakoulun Laskennallisen tekniikan laboratorion julkaisuja
Espoo 2006 REPORT B57

MODELING TRANSMITTERS, AMPLIFIERS AND NONLINEAR CIRCUITS FOR THE NEXT GENERATION OPTICAL NETWORKS

Jani Oksanen

TEKNILLINEN KORKEAKOULU
TEKNISKA HÖGSKOLAN
HELSINKI UNIVERSITY OF TECHNOLOGY
TECHNISCHE UNIVERSITÄT HELSINKI
UNIVERSITE DE TECHNOLOGIE D'HELSINKI

Helsinki University of Technology Laboratory of Computational Engineering Publications
Teknillisen korkeakoulun Laskennallisen tekniikan laboratorion julkaisuja
Espoo 2006 REPORT B57

MODELING TRANSMITTERS, AMPLIFIERS AND NONLINEAR CIRCUITS FOR THE NEXT GENERATION OPTICAL NETWORKS

Jani Oksanen

Dissertation for the degree of Doctor of Science in Technology to be presented with due permission of the Department of Electrical and Communications Engineering, Helsinki University of Technology, for public examination and debate in Auditorium TU 1 at Helsinki University of Technology (Espoo, Finland) on the 13^{th} of December, 2006, at 12 noon.

Helsinki University of Technology
Department of Electrical and Communications Engineering
Laboratory of Computational Engineering

Teknillinen korkeakoulu
Sähkö- ja tietoliikennetekniikan osasto
Laskennallisen tekniikan laboratorio

Distribution:
Helsinki University of Technology
Laboratory of Computational Engineering
P. O. Box 9203
FIN-02015 HUT
FINLAND
Tel. +358-9-451 4826
Fax. +358-9-451 4830
http://www.lce.hut.fi

Online in PDF format: http://lib.tkk.fi/Diss/2006/isbn9512283050

E-mail:Jani.Oksanen@tkk.fi

ISBN 951-22-8304-2 (printed)
ISBN 951-22-8305-0 (PDF)
ISSN 1455-0474

Picaset Oy
Helsinki 2006

HELSINKI UNIVERSITY OF TECHNOLOGY P. O. BOX 1000, FI-02015 TKK http://www.tkk.fi	ABSTRACT OF DOCTORAL DISSERTATION

Author Jani Oksanen

Name of the dissertation

Modeling transmitters, amplifiers and nonlinear circuits for the next generation optical networks

Date of manuscript 7.7.2006	Date of the dissertation 13.12.2006

☐ Monograph ☒ Article dissertation (summary + original articles)

Department	Department of Electrical and Communications Engineering
Laboratory	Laboratory of Computational Engineering
Field of research	optoelectronics
Opponent(s)	Prof. Claudio Mirasso
Supervisor (Instructor)	Prof. Jukka Tulkki

Abstract

In the current optical networks nonlinear interaction of optical signals with matter is often a nuisance in the operation of amplifiers, optical fibers and other linear devices. The next generation optical networks, on the other hand, need nonlinear optical components with signal processing capabilities. To create components that meet the demands of tomorrow, it is necessary to understand, control, exploit and enhance the available weak nonlinearities.

In this thesis the dynamic properties of quantum dot lasers and linear optical amplifiers are investigated. Additionally, optical memories and logic ports exploiting a new type of nonlinearity based on gain clamped optical amplifiers and interferometers are proposed. The properties of quantum dot lasers are studied by using a parametrized model for the bandstructure of the dots and the surrounding layers. The model is used to calculate the absorption spectrum, refractive index and other properties of the lasers at different excitation levels.

The properties of linear optical amplifiers, conventional gain clamped amplifiers and semiconductor optical amplifiers are described by a stochastic traveling wave rate equation model. The gain clamped optical amplifiers used together with interferometers are shown to provide a new fast nonlinearity, which can be used to construct coherent nonlinear optical circuits, including optical regenerators, flip-flop memories and logic gates.

The speed of the nonlinear devices presented in this thesis is limited by the modulation response of the gain clamped optical amplifiers above the laser threshold in the regime where there always is a large photon population in the laser mode. The speed may therefore reach values in excess of 100 GHz, or even higher values if the level of optical technologies evolves closer to the level of silicon technology. In principle the flip-flop structure developed in this thesis is suitable for integration.

Keywords semiconductor lasers and amplifiers, optical memories, nonlinear optical components

ISBN (printed) 951-22-8304-2	ISSN (printed) 1455-0474
ISBN (pdf) 951-22-8305-0	ISSN (pdf)
ISBN (others)	Number of pages 88 p.+app. 39 p.

Publisher Laboratory of Computational Engineering

Print distribution Laboratory of Computational Engineering

☒ The dissertation can be read at http://lib.tkk.fi/Diss/isbn9512283050

TEKNILLINEN KORKEAKOULU PL 1000, 02015 TKK http://www.tkk.fi	VÄITÖSKIRJAN TIIVISTELMÄ

Tekijä Jani Oksanen

Väitöskirjan nimi

Modeling transmitters, amplifiers and nonlinear circuits for the next generation optical networks

Käsikirjoituksen jättämispäivämäärä 7.7.2006	Väitöstilaisuuden ajankohta 13.12.2006

☐ Monografia ☒ Yhdistelmäväitöskirja (yhteenveto + erillisartikkelit)

Osasto	Sähkö- ja tietoliikennetekniikan osasto
Laboratorio	Laskennallisen tekniikan laboratorio
Tutkimusala	optoelektroniikka
Vastaväittäjä(t)	Prof. Claudio Mirasso
Työn valvoja	Prof. Jukka Tulkki
(Työn ohjaaja)	

Tiivistelmä

Optisten signaalien epälineaarinen vuorovaikutus väliaineen kanssa on usein ongelmallista optisten kuitujen, vahvistimien ja monien muiden optisten verkkojen komponenttien kannalta. Toisaalta seuraavan sukupolven optisissa verkoissa tarvitaan epälineaarisia signaalin käsittelyyn kykeneviä optisia komponentteja. Tulevaisuudessa tarvittavien komponenttien valmistamiseksi on tarpeen ymmärtää, hallita ja hyödyntää komponenteissa käytettyjen materiaalien heikkoja epälineaarisuuksia.

Tässä väitöskirjassa on tutkittu kvanttipistelasereiden ja lineaaristen optisten vahvistimien dynamiikkaa. Lisäksi on kehitetty ja mallinnettu uudentyyppisiä optisia muisteja sekä logiikkaportteja, joiden toiminta perustuu vahvistuslukittujen optisten vahvistimien ja interferometrien epälineaarisiin ominaisuuksiin. Kvanttipistelasereiden ominaisuuksia on tutkittu käyttämällä parametrisoitua vyörakennemallia, jossa on huomioitu kvanttipisteiden lisäksi myös ympäröivät materiaalikerrokset. Vyörakennemallia käyttäen on laskettu kvanttipistelaserin absorptio- ja taitekerroinspektri sekä laserin muita ominaisuuksia erilaisilla varauksenkuljettajien injektiotasoilla.

Lineaaristen optisten vahvistimien, perinteisten vahvistuslukittujen vahvistimien ja optisten puolijohdevahvistimien ominaisuuksia on kuvattu stokastisella etenevän aallon rate-yhtälömallilla. Koherenttien vahvistuslukittujen optisten vahvistimien käyttö yhdessä interferometrien kanssa mahdollistaa uudenlaisen nopean epälineaarisuuden, jonka avulla voidaan toteuttaa optisia piirejä kuten optisia regeneraattoreita, flip-flop muisteja ja logiikkaportteja.

Väitöskirjassa kuvattujen epälineaaristen piirien nopeutta rajoittaa optisten vahvistuslukittujen vahvistimien modulaationopeus laserointikynnyksen yläpuolella alueella, jossa laseroivassa moodissa on jatkuvasti suuri fotonipopulaatio. Siitä johtuen epälineaarisuus voi toimia yli 100 GHz nopeudella, tai jopa nopeammin optisen teknologian tason kehittyessä lähemmäs piiteknologian tasoa. Väitöskirjassa kehitetyt komponentit soveltuvat periaatteessa integroitaviksi.

Asiasanat puolijohdelaserit ja -vahvistimet,optiset muistit, epälineaariset optiset komponentit

ISBN (painettu) 951-22-8304-2	ISSN (painettu) 1455-0474
ISBN (pdf) 951-22-8305-0	ISSN (pdf)
ISBN (muut)	Sivumäärä 88 s.+liit. 39 s.

Julkaisija Laskennallisen tekniikan laboratorio

Painetun väitöskirjan jakelu Laskennallisen tekniikan laboratorio

☒ Luettavissa verkossa osoitteessa http://lib.tkk.fi/Diss/isbn9512283050

Preface

This thesis is a result of my attempt to dwell upon a few topics related to optical communications and data processing to learn more about optics and physics in general. The work has been conducted in the Laboratory of Computational Engineering (LCE) at Helsinki University of Technology (TKK) during the years 2001-2006. Funding for the work has been provided by the Graduate School in Electronics, Telecommunication and Automation (GETA) and the Academy of Finland. I also acknowledge the support of the Finnish Cultural Foundation, the Foundation of Commercial and Technical Sciences (Kaupallisten ja teknillisten tieteiden tukisäätiö) and the Foundation for Promoting Technology (Tekniikan edistämissäätiö).

Last but not least, I would like to express my gratitude to my supervisor, Prof. Jukka Tulkki, for patient guidance, encouragement and all the interesting relevant and unrelevant discussions over the years. I'm also indebted to my closest colleagues for offering a relaxed, inspiring and luminous working environment.

Otaniemi, 17th November 2006

Jani Oksanen

Contents

List of Publications

This thesis consists of an overview and of the following publications which are referred to in the text by their Roman numerals.

I J. Oksanen and J. Tulkki, *Linewidth enhancement factor and chirp in quantum dot lasers*, Journal of Applied Physics **94**, pp. 1983-1989 (2003).

II J. Oksanen and J. Tulkki, *On crosstalk and noise in an optical amplifier with gain clamping by vertical laser field*, IEEE Journal of Lightwave Technology **21**, pp. 1914-1919 (2003).

III J. Oksanen and J. Tulkki, *Fast 2R regeneration by coherent laser amplifiers*, IEEE Journal of Quantum Electronics **41**, pp. 1075-1082 (2005).

IV J. Oksanen and J. Tulkki, *Fast coherent all-optical flip-flop memory*, Applied Physics Letters **88**, pp. 181118-1-181118-3 (2006).

V J. Oksanen and J. Tulkki, *Fast all-optical flip-flop memory exploiting the electric field nonlinearity of coherent laser amplifiers*, IEEE Journal of Quantum Electronics **42**, pp. 509-516 (2006).

VI J. Oksanen and J. Tulkki, *Coherent optical logic by laser amplifiers with feedback*, accepted for publication in the IEEE Journal of Lightwave Technology **24** (2006).

Author's contribution

This dissertation is composed of six publications and an overview of the fundamental concepts occurring in them. J. Oksanen is the main author of all the publications. He has written the first drafts of the publications and performed all the simulations and calculations involved in them.

The main contribution of Prof. Tulkki has been the invaluable feedback throughout the process and the original idea for publication I.

List of Abbreviations

CW continuous wave

COFF coherent optical flip-flop

DBR distributed Bragg reflector

DFB distributed feedback

DOS density of states

EM electromagnetic

FP Fabry-Perot

FPA Fabry-Perot amplifier

GCSOA gain clamped semiconductor optical amplifier

LEF linewidth enhancement factor

LOA linear optical amplifier

NF noise figure

PGF probability generating function

QD quantum dot

QDL quantum dot laser

QW quantum well

QWL quantum well laser

SNR signal to noise ratio

SOA semiconductor optical amplifier

TE transverse electric

TM transverse magnetic

TWA traveling wave amplifier

VCSEL vertical cavity surface emitting laser

WDM wavelength division multiplexing

List of symbols

Γ	confinement factor
Φ	electric potential
Ψ	wave function
α	absorption
α_{km}	coherent state eigenvalue
α_{lef}	linewidth enhancement factor
β	spontaneous emission strength
γ_L	differential gain
γ_{abs}	absorption rate
γ_{st}	stimulated emission rate
$\delta_{n,m}$	Kronecker's delta
ε	permittivity
ε_0	permittivity of vacuum (8.854×10^{-12} As/Vm)
ε_r	relative permittivity
η	wave impedance ($\eta = \sqrt{\mu/\varepsilon}$)
κ	propagation direction
λ	wavelength
μ	permeability
μ_0	permeability of vacuum ($4\pi \times 10^{-7}$ Vs/Am)
μ_r	relative permeability
ν	envelope function of the $\mathbf{u}_{km}$
ξ	photon density = ξ | E-field $\|^2$ ($\xi = \sqrt{\varepsilon\mu^{-1}}/(2\hbar\omega c)$)
ρ	charge density
ρ_s	surface charge density
σ_{abs}	parameter for absorption strength
σ_{em}	parameter for emission strength
ς	relative standard deviation of QD energies
τ	carrier lifetime

τ_{cav}	lifetime of a photon in an optical cavity
ϕ	electron wave function
χ	electrical susceptibility
ω	angular frequency
$\mathbf{A}$	vector potential
$\hat{\mathbf{A}}$	vector potential operator
$\mathbf{B}$	magnetic flux density
$\hat{\mathbf{B}}$	magnetic flux density operator
C	amplification coefficient
$\mathbf{D}$	electric displacement field
$\mathbf{E}$	electric field
$\hat{\mathbf{E}}$	electric field operator
E_0	quantization energy
E_L	electric field phasor of a laser
E_{ext}	external electric field
E_b	bias electric field
E_g	band gap energy
E_{km}	strength of the normal mode $\mathbf{u}_{km}$
G	total amplification
$\mathcal{G}$	joint density of states
$\mathbf{H}$	magnetic field strength
$\hat{H}$	Hamilton operator
I_{eff}	effective injection current
$\mathbf{J}$	current density
$\mathbf{J}_s$	surface current density
K	spring constant
L	cavity length
$L\,()$	lifetime broadening
$\mathcal{L}$	Laplace transformation
$\mathbf{M}$	coupling matrix (also magnetization in chapter 2)

$\hat{M}$	photon measurement operator
$\hat{O}$	normal ordering operator
$\mathbf{P}$	polarization
P	optical power
$\hat{P}$	momentum quadrature operator
$\hat{Q}$	position quadrature operator
R	reflection coefficient
$\mathbf{S}$	Poynting vector
S	intensity of an EM field
T	sampling time
$T_{L,s}$	effective mirror transmission coefficients
$\hat{W}_{\text{abs}}$	absorption rate operator
$\hat{W}_{\text{em}}$	emission rate operator
W_{ext}	injection rate of externally injected photons
W_{if}	transition rate from state i to state f
W_{inj}	injection rate
W_{nst}	transition rate excluding stimulated emission
W_{sp}	spontaneous emission rate into the cavity mode
$\hat{a}^\dagger$	creation operator
$\hat{a}$	annihilation operator
c	speed of light
c_0	speed of light in vacuum (2.998×10^8 m/s)
e	elementary charge (1.602×10^{-19} C)
f	frequency
f_v, f_c	Fermi distribution of the valence/conduction band
g	gain
h	Planck's constant (6.626×10^-34 Js)
$\hbar$	Dirac's constant (1.055×10^-34 Js)
$\mathbf{k}$	wave vector
k	wavenumber

k_0	wavenumber in free space
m	mass
m_0	free electron mass (9.109$\times 10^{-31}$ kg)
$\hat{n}$	photon number operator
$n_{\delta e}$	small signal carrier density
$n_{\delta L}$	small signal photon density
n_L	photon density
n_{L0}	steady state photon density
n_e	electron (carrier) density
n_{e0}	steady state carrier density
$\overline{n}_{km}$	average value of the photon number in mode km
n_r	refractive index
n_{ri}	imaginary part of the complex refractive index
$\hat{p}$	momentum operator
$\mathbf{p}_{mn}^{\mathbf{u}}$	momentum matrix element along $\mathbf{u}$
s	Laplace transformation variable
$s_{i,\kappa}$	signal mode photon density
$t_{A,B,C,a,b}$	waveguide transmission coefficient
$\mathbf{u}_\omega$	Fourier component of the electric field at frequency ω
$\mathbf{u}_{km}(\mathbf{r})$	normal mode km
w_E	energy density of an EM field
$\hat{x}$	position operator

1 Introduction

The first laser was developed and demonstrated by the American physicist Theodore Maiman in 1960. He succeeded in optically pumping a ruby crystal into a population inverted state and in creating favorable conditions for lasing [1]. His work was preceded by theoretical predictions of how to extend the operating range of masers into the optical domain, and of course, the maser technology itself [2]. The demonstration of a working laser revived rapid progress in optics and gave birth to a new field concentrating on the study of lasers, waveguides and nonlinear optical phenomena.

The availability of lasers gave researchers inspiration and a new tool to create intense and coherent monochromatic optical beams. New discoveries and demonstrations on the nonlinear effects in different materials emerged at a very impressive pace in the 1960s. Soon after Maiman, a research group in Bell Laboratories developed the first gas laser using a mixture of helium and neon as the lasing medium and several groups reported stimulated emission in homojunction gallium arsenide diodes [3–5]. Second harmonic generation in crystalline quartz, the ascertainment of stimulated Raman and Brillouin scattering and many other nonlinear effects in optical fibers were also demonstrated in the 60s [6–9].

In optical communications, the development of optical fibers has had at least as crucial a role as the development of optical transmitters and receivers. Total reflection of light in general was observed and understood already in the 19th century and elementary fibers without the cladding were fabricated as early as in the 1920s. In the 1950s the use of a cladding layer around the glass core led to the optical fiber structures primarily used today [10]. Since then the evolution of the optical fiber technology has been driven by the development of the manufacturing process, materials and the profiles of the core and the cladding. The ability to significantly reduce the amount of water molecules and other impurities in the fibers reduced the losses of optical fibers to a level of 0.2 dB/km and close to the fundamental limit of Rayleigh scattering by the end of 1970s [11]. It also made the nonlinear effects, which are primarily a nuisance in point to point links, in the long fibers better noticeable. An equally important, and not only technical, advancement was

the introduction of rare earth elements, especially erbium, as a dopant in the core of the fibers in the late 1980s. They made fiber amplifiers possible and enabled even longer span for the optical links without using electronics. More recently photonic crystal technology has also been introduced in optical fibers.

The huge transmission capacity, long link lengths and the minimal interference with the outside world offered by the optical technology were successfully taken into full use in the backbone of the commercial communications networks in an ever accelerating pace in the 1990s. However, optical networks of today still employ conceptionally very simple linear optical devices like quantum well lasers, optical fibers, fiber amplifiers, filters and add and drop multiplexers. Any complex operations such as switching, logic, regeneration and memory are still handled by electronics and require converting the signal from optical to electronic form and back.

The undisputed victory of optical fibers over copper cables as a transmission medium is diminished only by the current inability of optical technologies to practically perform the nonlinear complex operations. The electro-optic conversions required in the optical networks are clumsy and costly and replacing the electronic components with optical solutions that can tap into the enormous bandwidth of optical signals has been intensively researched and expected. No cost effective optical alternatives for the electronic components exist at the moment [12, 13].

Device prototypes demonstrated to this date have been able to reproduce most of the functions needed in the next generation optical networks involving purely optical components. However, the prototypes do not yet meet *all* the requirements of practical commercial switches, memories, delay lines, regenerators or logic gates. These requirements can be summarized by compactness and suitability for integration, fast or extremely fast operation, acceptable power consumption, stability under various operating conditions and good tolerance for noise. In switching applications one would additionally hope for good scalability and transparency.

The publications included in this thesis relate to the nonlinear components, transmitters and amplifiers that could be used in the future optical networks. Publications I and II concentrate on quantum dot lasers and gain clamped semiconductor optical am-

plifiers, linear components with superior properties compared to the traditional lasers and amplifiers. Publications III through VI exploit the properties of the gain clamped laser amplifiers, phase locking and interferometers in creating a new form of nonlinearity. The nonlinearity is used to generate all-optical regenerators, logic functions and flip-flop circuits with many desirable properties. The summary part of the thesis gives a brief overview of the physics and topics encountered in the publications: the properties of light, its interaction with matter, the principles of laser operation and light amplification and the principle of using interferometry with gain clamped amplifiers to generate a new nonlinearity that lends a hand for new coherent nonlinear devices.

2 Properties of light

Light is electromagnetic (EM) radiation in the frequency range covering the visible, ultraviolet and infrared frequencies (Fig. 2.1). The behaviour of light is usually described by three models of increasing complexity and accuracy: ray optics, wave optics and quantum optics. The fundamental equations of the wave and quantum optical descriptions frequently encountered in preparation of this thesis are summarized in the following sections. The given presentation aims at briefly reviewing the key concepts and formulas of the theory. For a detailed derivation of the results, the reader is referred to for example [14–16].

2.1 Classical field theory

The classical theory of electromagnetism was combined and completed by James Maxwell in 1873. The classical EM field is characterized by the electric and magnetic fields associated with it. Both fields are vector quantities with well defined values.

In vector form Maxwell's equations describe concisely and accurately the behaviour of EM waves, when the quantum nature of the field can be neglected. The four Maxwell's equations are [14]

$$\nabla \times \mathbf{E}(\mathbf{r},t) = -\dot{\mathbf{B}}(\mathbf{r},t) \tag{2.1}$$

$$\nabla \times \mathbf{H}(\mathbf{r},t) = \dot{\mathbf{D}}(\mathbf{r},t) + \mathbf{J}(\mathbf{r},t) \tag{2.2}$$

$$\nabla \cdot \mathbf{D}(\mathbf{r},t) = \rho(\mathbf{r},t) \tag{2.3}$$

$$\nabla \cdot \mathbf{B}(\mathbf{r},t) = 0 \tag{2.4}$$

where $\mathbf{E}$ is the electric field, $\mathbf{H}$ the magnetic field strength, $\mathbf{D}$ the electric displacement field, $\mathbf{B}$ the magnetic flux density, $\mathbf{J}$ the free current density and ρ the free charge density. The time derivatives are indicated by the dots above the symbols. In linear isotropic media the relations between the fields are given by the constitutive equations

$$\mathbf{D} = \varepsilon_r \varepsilon_0 \mathbf{E} = \varepsilon_0 \mathbf{E} + \mathbf{P} \tag{2.5}$$

$$\mathbf{B} = \mu_r \mu_0 \mathbf{H} = \mu_0 (\mathbf{H} + \mathbf{M}) \tag{2.6}$$

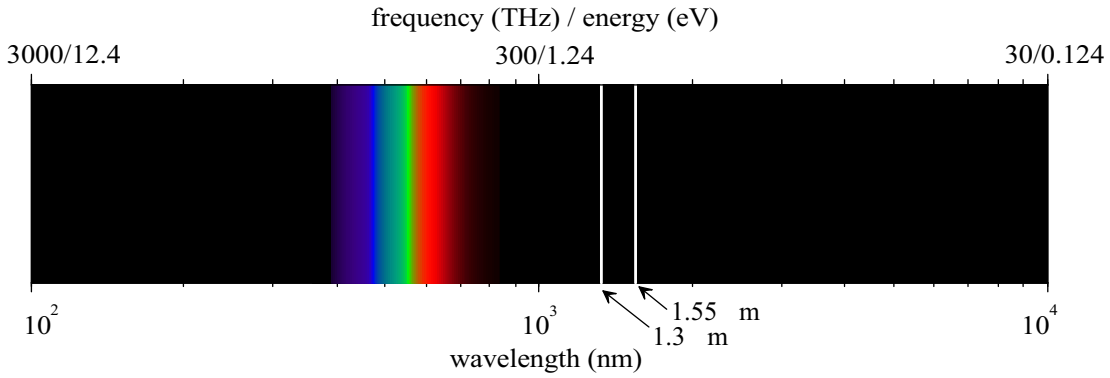

Figure 2.1: The communications wavelengths in the electromagnetic spectrum of light. The spectrum of visible light (indicative) has shorter wavelengths than the most commonly used communications wavelengths, located at 1.3 μm and 1.55 μm. The far infrared (up to wavelengths ~ 1 mm) is not included in the spectrum.

where $\mathbf{P}$ is the polarization and $\mathbf{M}$ the magnetization of the material. The relative electrical permittivity ε_r and the relative magnetic permeability μ_r in Eqs. (2.5)-(2.6) are generally frequency dependent tensors of rank two. In this thesis only materials which are effectively isotropic and optically inactive are considered and hence scalar values are assumed for ε_r and μ_r. The boundary conditions at the boundary of two materials, 1 and 2, are $\mathbf{n}\times\mathbf{E}_1 = \mathbf{n}\times\mathbf{E}_2$, $\mathbf{n}\cdot\mathbf{D}_1 - \mathbf{n}\cdot\mathbf{D}_2 = \rho_s$, $\mathbf{n}\times\mathbf{H}_1 - \mathbf{n}\times\mathbf{H}_2 = \mathbf{J}_s$ and $\mathbf{n}\cdot\mathbf{B}_1 = \mathbf{n}\cdot\mathbf{B}_2$, where $\mathbf{n}$ is a unit vector normal to the boundary and pointing to material 1, and ρ_s and $\mathbf{J}_s$ are the surface charge and current densities, respectively.

In dealing with the theory of electromagnetism it is often useful to define two auxiliary functions, the scalar potential $\Phi(\mathbf{r},t)$ and the vector potential $\mathbf{A}(\mathbf{r},t)$ defined by the equations [17]

$$\mathbf{E}(\mathbf{r},t) = -\nabla\Phi(\mathbf{r},t) - \dot{\mathbf{A}}(\mathbf{r},t) \tag{2.7}$$

$$\mathbf{B}(\mathbf{r},t) = \nabla\times\mathbf{A}(\mathbf{r},t)\,. \tag{2.8}$$

The choice of $\mathbf{A}$ is ambiguous. Although the selected gauge does not affect the physical solution of the problem, it may result in simpler algebra. In static problems it is common to use the Coulomb gauge and choose $\nabla\cdot\mathbf{A} = 0$ whereas in magnetodynamics it is customary to use the Lorenz gauge where $\nabla\cdot\mathbf{A} = -\mu\varepsilon\partial\Phi/\partial t$.

2.1.1 Wave equation

For many purposes of linear optics one can reduce the four Maxwell's equations into a single equation for the electric field (or the magnetic field, vector potential or scalar potential). If μ and ε are assumed constants or piecewise constants, taking the curl of both sides of Eq. (2.1) and using the constitutive equations and the vector identity $\nabla \times \nabla \times \mathbf{f} = \nabla (\nabla \cdot \mathbf{f}) - \nabla^2 \mathbf{f}$ gives the nonhomogeneous wave equation:

$$\nabla^2 \mathbf{E}(\mathbf{r}, t) - \mu\varepsilon \ddot{\mathbf{E}}(\mathbf{r}, t) = \nabla \frac{\rho(\mathbf{r}, t)}{\varepsilon} + \mu \dot{\mathbf{J}}(\mathbf{r}, t). \tag{2.9}$$

Setting the free charges and currents to zero reduces Eq. (2.9) into the homogeneous wave equation

$$\nabla^2 \mathbf{E}(\mathbf{r}, t) - \mu\varepsilon \ddot{\mathbf{E}}(\mathbf{r}, t) = 0. \tag{2.10}$$

The homogeneous wave equation (2.10) is satisfied by any function of the form $\mathbf{f}(\mathbf{k} \cdot \mathbf{r} - \omega t)$ where

$$k = \sqrt{\mu\varepsilon}\omega \tag{2.11}$$

and ω is the angular frequency, $k = \sqrt{k_x^2 + k_y^2 + k_z^2}$ is the wave number and k_x, k_y and k_z are the x, y and z -components of the wave vector $\mathbf{k}$ of the wave. Also functions of the form $\mathbf{f}(\mathbf{k} \cdot \mathbf{r} + \omega t)$ are solutions to (2.10) with $k = -\sqrt{\mu\varepsilon}\omega$, but then the direction of propagation of the wave would have to be along $-\mathbf{k}$, instead of the customary $\mathbf{k}$. By Fourier transforming the electric field in the homogeneous wave equation (2.10), one obtains the Helmholtz equation

$$\nabla^2 \mathbf{u}_\omega(\mathbf{r}) + \mu\varepsilon\omega^2 \mathbf{u}_\omega(\mathbf{r}) = 0 \tag{2.12}$$

where $\mathbf{u}_\omega$ are the Fourier components of the electric field. Using (2.11) in the Helmholtz equation gives the eigenvalue equation

$$\nabla^2 \mathbf{u}_{km}(\mathbf{r}) + k^2 \mathbf{u}_{km}(\mathbf{r}) = 0 \tag{2.13}$$

where m indexes the different eigenvalues bound to the fixed wave number k. The eigenfunctions $\mathbf{u}_{km}(\mathbf{r})$ are called the normal modes of the field. The normal modes are orthogonal and normalized to satisfy $\int \mathbf{u}_{km}(\mathbf{r}) \cdot \mathbf{u}_{k'm'}(\mathbf{r})\, d^3r = \delta_{k,k'}\delta_{m,m'}$. They also depend on the boundary conditions of the problem.

Physically the general solution $\mathbf{f}(\mathbf{k}\cdot\mathbf{r}-\omega t)$ of the homogeneous wave equation (2.10) describes a wave that propagates along $\mathbf{k}$ with a phase velocity $c=\omega/k=1/\sqrt{\mu\varepsilon}$. In vacuum the velocity of light is a natural constant $c_0=1/\sqrt{\mu_0\varepsilon_0}$, and inside matter the velocity is given by $c=c_0/n_r$ where the refractive index n_r is correspondingly $n_r=\sqrt{\varepsilon_r\mu_r}$ (typically $n_r\sim 3$ for common semiconductors). When there are no free charges and the permittivity and permeability of the material are constant, the solutions of the wave equation are plane waves of the form $\mathbf{E}(\mathbf{r},t)=e^{i\mathbf{k}\cdot\mathbf{r}}e^{-i\omega t}$ where $|\mathbf{k}|=k$ and m indexes the direction of $\mathbf{k}$. From Maxwell's equations it then follows that $\mathbf{k}$ and $\mathbf{u}_{km}$ are perpendicular to each other and $\mathbf{H}$ is perpendicular to both $\mathbf{k}$ and $\mathbf{E}$ if there are no free currents. Furthermore, the magnitude of $\mathbf{H}$ can be obtained from $H=E/\eta$, where $\eta=\sqrt{\mu/\varepsilon}$ is the wave impedance.

The intensity S of an EM wave is expressed by the Poynting vector [14]

$$\mathbf{S}(\mathbf{r},t)=\mathbf{E}(\mathbf{r},t)\times\mathbf{H}(\mathbf{r},t). \tag{2.14}$$

For harmonic EM fields propagating in homogeneous media the average magnitude of the Poynting vector is

$$S(\mathbf{r})=\frac{1}{2\eta}E(\mathbf{r})^2 \tag{2.15}$$

where $E(\mathbf{r})$ is the magnitude of the electric field at $\mathbf{r}$. The energy density w_E of the EM field is given by

$$w_E = \frac{\varepsilon}{2}|\mathbf{E}(\mathbf{r},t)|^2+\frac{\mu}{2}|\mathbf{H}(\mathbf{r},t)|^2. \tag{2.16}$$

When free charges or currents are present, the inhomogeneous wave equation (2.9) must be used to describe the propagation of the wave. For harmonic signals (or Fourier components of the signal) it then becomes useful to generalize the solutions of the homogeneous case so that imaginary values of the wave vector k and the material permittivity ε are used to account for the light–matter interaction. The plane wave can then be written in the form $\mathbf{u}_{km}(\mathbf{r})=e^{i\mathbf{k}\cdot\mathbf{r}}=e^{i\Re\{\mathbf{k}\}\cdot\mathbf{r}}e^{-\Im\{\mathbf{k}\}\cdot\mathbf{r}}$, where $\Re$ denotes the real part and $\Im$ denotes the imaginary part.

The absorption loss α is defined as the relative change of the intensity along the propagation path by

$$\alpha = -\frac{\partial S(\mathbf{r},t)}{S(\mathbf{r},t)\,\partial r_k}, \tag{2.17}$$

where the derivative is taken along the direction of propagation. The connection of the absorption and the refractive index to the complex permittivity and permeability of the material is given by

$$\alpha = 2\Im\{k\} = 2\omega\Im\{\sqrt{\varepsilon\mu}\}/c_0 = 2k_0\Im\{\sqrt{\varepsilon_r\mu_r}\} = 2k_0 n_{ri} \tag{2.18}$$

$$n_r = \Re\{\sqrt{\varepsilon_r\mu_r}\} \tag{2.19}$$

where $n_{ri} = \Im\left\{\sqrt{\varepsilon_r\mu_r}\right\}$ is imaginary part of the complex refractive index and k_0 is the wave number in vacuum ($\varepsilon = \varepsilon_0$ and $\mu = \mu_0$).

2.1.2 Kramers-Kronig relations

The Kramers-Kronig –relations link together the spectra of the real and imaginary parts of complex functions that have no poles in the upper (or lower) complex plane and for which $f(-\omega) = f^\star(\omega)$. In optics they are often used to link together the refractive index $n_r(\omega)$ (proportional to the real part of k) and the absorption $\alpha(\omega)$ (proportional to the imaginary part of k) by the relations [18, 19]

$$n_r(\omega) = 1 + \frac{c}{\pi}P\int_0^\infty \frac{\alpha(\omega')}{\omega'^2-\omega^2}d\omega' \tag{2.20}$$

$$\alpha(\omega) = -4\frac{\omega^2}{c\pi}P\int_0^\infty \frac{n_r(\omega')-1}{\omega'^2-\omega^2}d\omega' \tag{2.21}$$

where $P\int$ denotes the principal value of the integral.

The relations provide a tool for evaluating the change in the refractive index if the absorption spectrum changes. This is particularly useful in evaluating the linewidth enhancement factor in semiconductor lasers.

2.1.3 Linewidth enhancement factor

The linewidth enhancement factor (LEF) describes how the refractive index of the material changes along with the carrier density. It is defined as the ratio of the change in real

and imaginary parts n_r and n_{ri} of the complex refractive index [20]

$$\alpha_{\text{lef}}(\hbar\omega) = \frac{\Delta n_r(\hbar\omega)}{\Delta n_{ri}(\hbar\omega)} = -2k_0 \frac{\partial n_r(\hbar\omega)}{\partial \alpha(\hbar\omega)}. \tag{2.22}$$

In addition of being related to the chirp in optical components, the linewidth of continuous wave (CW) semiconductor lasers is also increased by a factor $1 + \alpha_{\text{lef}}^2$ with respect to gas lasers, for which $\alpha_{\text{lef}} \approx 0$.

2.2 Quantized electro-magnetic field

In a more fundamental treatment, the EM field must be described as a quantum field. The field quanta are called photons and they are bosonic particles with zero rest mass [15, 21]. In this thesis, quantum theory of light is mainly needed for better understanding of some fundamental concepts of optics, particularly the interaction with matter and the noise analysis of publication II.

To show the analogy between the quantum field and the harmonic oscillator, the electric field in the classical homogeneous wave equation (2.10) is first written as

$$\mathbf{E}(\mathbf{r}, t) = \sum_{k,m} E_{km}(t)\, \mathbf{u}_{km}(\mathbf{r}). \tag{2.23}$$

For now $E_{km}(t)$ are assumed to be real functions and denote the strength of the normal mode km. The normal modes $\mathbf{u}_{km}$ are assumed real as well and satisfy (2.13). The homogenous wave equation for each km simplifies into

$$k^2 E_{km}(t) - \mu\varepsilon \ddot{E}_{km}(t) = 0. \tag{2.24}$$

This equation is identical in form with the equation of motion of a classical harmonic oscillator. Experiments and more extensive theories have shown that this analogy extends all the way to the quantum theory and it is straightforward to apply the properties of the quantum mechanical harmonic oscillator to the EM oscillator.

The Schrödinger equation of the simple harmonic oscillator is [22]

$$\hat{H}_{SHO}\Psi = i\hbar \frac{d}{dt}\Psi \tag{2.25}$$

with the Hamiltonian $\hat{H}_{SHO}$ given by

$$\hat{H}_{SHO} = \frac{\hat{p}^2}{2m} + \frac{K\hat{x}^2}{2}. \tag{2.26}$$

The harmonic oscillator is characterized by the mass m of the oscillator and the spring constant K. Terms $\hat{p}$ and $\hat{x}$ are the momentum and position operators, respectively. The eigenvalue spectrum of the Schrödinger equation for $\hat{H}_{SHO}$ is discrete and the energy eigenvalues are given by $E_n = (n + 1/2)\,\hbar\omega$ where $\omega = \sqrt{K/m}$.

The eigenstates $|n>$ of the Hamiltonian $\hat{H}_{SHO}$ can be obtained recursively from each others by using the creation and annihilation operators $\hat{a}^\dagger$ and $\hat{a}$ and their properties $\hat{a}^\dagger|n>=\sqrt{n+1}|n+1>$ and $\hat{a}|n>=\sqrt{n}|n-1>$. The operators $\hat{a}^\dagger$, $\hat{a}$, $\hat{x}$ and $\hat{p}$ and the commutator $\left[\hat{a}, \hat{a}^\dagger\right]$ (defined for two arbitrary operators $\hat{D}$ and $\hat{F}$ by $\left[\hat{D}, \hat{F}\right] = \hat{D}\hat{F} - \hat{F}\hat{D}$) have the following properties and relations [22]:

$$\hat{a} = \sqrt{\frac{m\omega}{2\hbar}}\hat{x} + i\frac{\hat{p}}{\sqrt{2m\omega\hbar}} \tag{2.27}$$

$$\hat{a}^\dagger = \sqrt{\frac{\varepsilon}{2\hbar\omega}}\hat{x} - i\sqrt{\frac{\omega}{2\varepsilon\hbar}}\hat{p} \tag{2.28}$$

$$\hat{x} = \sqrt{\frac{\hbar}{2m\omega}}\left(\hat{a} + \hat{a}^\dagger\right) \tag{2.29}$$

$$\hat{p} = i\sqrt{\frac{m\omega\hbar}{2}}\left(\hat{a}^\dagger - \hat{a}\right) \tag{2.30}$$

$$\left[\hat{a}, \hat{a}^\dagger\right] = 1. \tag{2.31}$$

The analogy of the equation of motion of the classical harmonic oscillator and Eq. (2.24) for the normal mode km on one hand and of the energy of the harmonic oscillator and the energy of the EM field (2.16) on the other suggest substituting the mass, the spring constant and position of the classical oscillator with

$$m \leftrightarrow \varepsilon/\omega_{km}^2 \tag{2.32}$$

$$K \leftrightarrow \varepsilon \tag{2.33}$$

$$\hat{x} \leftrightarrow \hat{E}_{km} \tag{2.34}$$

in Eqs. (2.25)-(2.31) when dealing with EM oscillators.

Substituting (2.32)-(2.34) in Eqs. (2.29) and (2.23) and generalizing for complex $\mathbf{u}_{km}$ gives the electric field operator of an EM field as [15]

$$\hat{\mathbf{E}} = \sum_{k,m} \sqrt{\frac{\hbar\omega_{km}}{2\varepsilon}} \left(\mathbf{u}^{\star}_{km}(\mathbf{r})\, \hat{a}^{\dagger}_{km} + \mathbf{u}_{km}(\mathbf{r})\, \hat{a}_{km} \right). \tag{2.35}$$

The expectation value of the electric field of a normal mode km in state $|n_{km}>$ is then obtained from $< n_{km}|\hat{\mathbf{E}}|n_{km}>$. The sinusoidal time dependence of the electric field arises from the time dependence of the state vectors in the Schrödinger picture ($|n_{km}> \sim e^{i\omega t}$) or of the time dependence of the operators $\hat{a}^{\dagger}$ ($\sim e^{i\omega t}$) and $\hat{a}$ ($\sim e^{-i\omega t}$) in the Heisenberg picture. The magnetic field and the vector potential are represented by the operators [15]

$$\hat{\mathbf{B}} = \sum_{k,m} i\sqrt{\frac{\hbar}{2\varepsilon\omega_{km}}} \left(\nabla \times \mathbf{u}^{\star}_{km}(\mathbf{r})\, \hat{a}^{\dagger}_{km} - \nabla \times \mathbf{u}_{km}(\mathbf{r})\, \hat{a}_{km} \right) \tag{2.36}$$

$$\hat{\mathbf{A}} = \sum_{k,m} i\sqrt{\frac{\hbar}{2\varepsilon\omega_{km}}} \left(\mathbf{u}^{\star}_{km}(\mathbf{r})\, \hat{a}^{\dagger}_{km} - \mathbf{u}_{km}(\mathbf{r})\, \hat{a}_{km} \right). \tag{2.37}$$

Other important operators in the quantized EM field description are the position and momentum quadrature operators $\hat{Q}$ and $\hat{P}$ which are related to the creation and annihilation operators by the relations [21, 23]

$$\hat{Q} = \sqrt{\frac{\hbar}{2\omega_{km}}} \left(\hat{a}_{km} + \hat{a}^{\dagger}_{km} \right) \tag{2.38}$$

$$\hat{P} = -i\sqrt{\frac{\hbar\omega_{km}}{2}} \left(\hat{a}_{km} - \hat{a}^{\dagger}_{km} \right). \tag{2.39}$$

2.2.1 Fock states and Glauber states

Two alternative basis are most often used to represent the state of an electromagnetic field. The eigenstates $|n_{km}>$ of the photon number operator $\hat{n}_{km} = \hat{a}^{\dagger}_{km}\hat{a}_{km}$ of the normal mode km are called Fock states or photon number states and satisfy the eigenvalue equation [16, 23]

$$\hat{n}_{km}|n_{km}> = n_{km}|n_{km}> \tag{2.40}$$

while the eigenstates $|\alpha_{km}>$ of the annihilation operator $\hat{a}_{km}$ are called Glauber states or coherent states and satisfy

$$\hat{a}_{km}|\alpha_{km}> = \alpha_{km}|\alpha_{km}> . \tag{2.41}$$

In pure Glauber states the electric and magnetic fields have a well defined amplitude and phase in the classical limit $|\alpha_{km}|^2 \gg 1$ where $E_{km} \approx \sqrt{2\hbar\omega/\varepsilon}\alpha_{km}$. The light generated by high quality lasers corresponds closely to pure Glauber states.

Any Glauber state can be represented in the Fock state basis by [16, 23]

$$|\alpha_{km}>= e^{-|\alpha_{km}|^2/2} \sum_{n=0}^{\infty} \frac{\alpha_{km}^n}{\sqrt{n!}}|n> \tag{2.42}$$

and the probability p_n of there being n photons in the state $|\alpha_{km}>$ is given by

$$p_n = |<n|\alpha_{km}>|^2 = e^{-|\alpha_{km}|^2} \frac{|\alpha_{km}|^{2n}}{n}. \tag{2.43}$$

The energy of the normal mode km for a Fock state $|n_{km}>$ or a Glauber state $|\alpha_{km}>$ is

$$E_{km} = \left(\frac{1}{2} + n_{km}\right)\hbar\omega = \left(\frac{1}{2} + |\alpha_{km}|^2\right)\hbar\omega. \tag{2.44}$$

In addition to the coherent states, a commonly encountered photon state is the chaotic state created by a thermal source. In Fock basis the chaotic state $|\xi_{km}>$ can be represented as [16]

$$|\xi_{km}>= \sum_n \frac{\overline{n}_{km}^n}{(1+\overline{n}_{km})^{1+n}}|n> \tag{2.45}$$

where $\overline{n}_{km}$ is the average number of photons contained in the normal mode km. Chaotic states differ from the Fock and Glauber states in the property that even for $\overline{n}_{km} \gg 1$ the maximum of the probability distribution $p_n = |<\xi_{km}|n_{km}>|^2$ is located at $n = 0$.

2.2.2 Light-matter interaction

According to the Fermi golden rule (FGR), arising from the time dependent perturbation theory, the transition rate W_{if} from an initial state $|i>$ to a final state $|f>$ due to a harmonic perturbation H' at an angular frequency ω is given by [24]

$$W_{if} = \frac{2\pi\left|\langle f|H'|i\rangle\right|^2}{\hbar} L\left(\hbar\omega_{fi} \pm \hbar\omega\right) \tag{2.46}$$

where $L\left(\hbar\omega_{fi} \pm \hbar\omega\right)$ is the probability distribution of $\hbar\omega_{fi}$ (usually Dirac delta function or a Lorenz-distribution). The transition energy is given by $\hbar\omega_{fi} = (E_f - E_i)$ with E_f and E_i being the energies of the final and initial states. The + sign in the probability distribution is for emission and - for absorption.

For optical excitations it is convenient to write the states of the system as a direct product of the electronic $|\phi>$ and optical states $|n>$, in the form $|f>=|\phi_f>|n>$. The absorption W_{if}^{abs} and emission W_{if}^{em} rates for a single optical mode km with n_{pi} initial photons, Hamiltonian $\hat{H}' = e\hat{\mathbf{p}}\cdot\hat{\mathbf{A}}_{km}/m_0$ and $\hat{\mathbf{A}}_{km}$ given by Eq. (2.37) can be calculated from [24]

$$W_{if}^{\text{abs}}(\omega) = \frac{\pi e^2 n_{pi}}{\varepsilon\omega m_0^2}\left|<\phi_f|\hat{\mathbf{p}}\cdot\mathbf{u}(\mathbf{r})|\phi_i>\right|^2 L(\hbar\omega_{fi}-\hbar\omega) \tag{2.47}$$

$$\begin{aligned} W_{if}^{\text{em}}(\omega) &= W_{if}^{\text{stim}}(n_i)+W_{if}^{\text{sp}} = \frac{\pi e^2(n_{pi}+1)}{\varepsilon\omega m_0^2}\left|<\phi_f|\hat{\mathbf{p}}\cdot\mathbf{u}(\mathbf{r})|\phi_i>\right|^2 \\ &\times L(\hbar\omega_{fi}+\hbar\omega) \end{aligned} \tag{2.48}$$

where emission occurs by stimulated emission W_{if}^{stim} [the term proportional to n_{pi} in (2.48)] and spontaneous emission W_{if}^{sp} [the term independent of n_{pi} in (2.48)].

The macroscopic absorption coefficient of a material can be obtained from the rate of absorption and stimulated emission by summing over all the possible initial and final electronic states and weighting by the corresponding probability of the initial state being occupied (p_i) and the final state being available ($1-p_f$). The absorption for a linearly polarized plane wave with polarization along the vector $\mathbf{u}$ becomes [24]

$$\begin{aligned} \alpha(\hbar\omega) &= \frac{\pi e^2}{\varepsilon_0\omega c_0 n_r m_0^2}\sum_{f,i}\left|<\phi_f|\hat{\mathbf{p}}\cdot\mathbf{u}(\mathbf{r})|\phi_i>\right|^2 \\ &\times L(\hbar\omega_{fi}-\hbar\omega)(p_i-p_f). \end{aligned} \tag{2.49}$$

In III-V compound semiconductors the final and initial electronic states are defined by the band, spin and electron wave vector. If the semiconductor is in thermal quasi-equilibrium, the probabilities p_i and p_f can be calculated from the quasi-Fermi distributions $f_{c,v}(E) = \left\{1+\exp\left[\left(E-E_f^{c,v}\right)/k_BT\right]\right\}^{-1}$ where $E_f^{c,v}$ are the quasi-Fermi levels of the conduction and valence bands, respectively [19]. The absorption of a semiconductor within the parabolic band approximation is given by

$$\begin{aligned} \alpha(\hbar\omega) &= \frac{\pi e^2}{\varepsilon_0\omega c_0 n_r m_0^2 V}\sum_{m,n}\Gamma^2\left|\mathbf{p}_{mn}^{\mathbf{u}}\right|^2\int_0^\infty dE\,\mathcal{G}(E)L(E-\hbar\omega) \\ &\times [f_v(E_v)-f_c(E_c)]. \end{aligned} \tag{2.50}$$

The momentum matrix element $|\mathbf{p}_{mn}^{\mathbf{u}}|$ ($\sim 10^{-24}$ kgm/s for typical semiconductors) is evaluated over the unit cell for the initial band n and final band m and for light polarization

along $\mathbf{u}$. The overlap of the electronic envelope functions Ψ_f and Ψ_i with the envelope function $\nu_{km}(\mathbf{r})$ of the normal electric field mode gives rise to the confinement factor $\Gamma = |<\Psi_f|\nu(\mathbf{r})|\Psi_i>|$. If $\Gamma = 1$ it is customary to speak of the material gain in distinction to modal gain. Summation over m and n is over the sub bands of the valence and conduction bands (if applicable) and the transition energy E of the electronic state is contributed to the valence (E_v) and conduction (E_c) bands according to the requirement of preserving the electron wave vector in the transition. The joint density of states $\mathcal{G}$ is the density of states for the initial – final state pairs that are possible for transitions that preserve the wave vector [19]. The differences in the characteristics of the absorption spectrum of bulk, quantum well and quantum dot materials is primarily manifested by the different forms of the joint density of states.

2.3 Noise

2.3.1 Figures of merit for noise

An optical signal $s(t)$ can be represented as a sum of the actual signal power $s_0(t)$ and an additional noise signal $s_n(t)$ in the form

$$s(t) = s_0(t) + s_n(t). \tag{2.51}$$

The noise can be statistically described by the variance and the optical signal to noise ratio (SNR_{opt}) of the signal by [17]

$$Var[s(t)] = \overline{\left[s(t) - \overline{s(t)}\right]^2} = \overline{s(t)^2} - \overline{s(t)}^2 \tag{2.52}$$

$$SNR_{\text{opt}}[s(t)] = \frac{\overline{s(t)}}{\sqrt{Var[s(t)]}} \tag{2.53}$$

where the overbar denotes the time average over sampling time T. Optical signals, and noise, however, are usually measured using electrical components in which the generated current is proportional to the optical power and electric power is proportional to the square of the optical power in the normal operating regime. Therefore it is customary to use the electrical signal to noise ratio (SNR) for optical signals as well (compare for example [17]

and [25]):

$$SNR = SNR_{\text{opt}}^2 = \frac{\overline{s\left(t\right)}^2}{Var\left[s\left(t\right)\right]}. \tag{2.54}$$

A figure of merit for the amount of noise in optical amplifiers is the noise figure (NF), defined by using the SNR at the input and at the output of the amplifier [26]

$$NF = \frac{SNR_{\text{in}}}{SNR_{\text{out}}}. \tag{2.55}$$

2.3.2 Photon detection

Photon detection is based on measuring the current generated by light in semiconductors. Different semiconductor device configurations ranging from photoconductors to photodiodes and phototransistors can be used for this purpose [17]. The noise in the measured signal is composed of the noise present in the original optical signal and the noise generated in the detector itself. Only the noise directly related to optical signals is considered here.

Starting from the Fermi golden rule (2.46) the absorption and emission rates (2.47) and (2.48) were obtained. The quantum mechanical absorption and emission rate operators for constant excitation with optical pumping or electrical injection can be correspondingly written for a single normal mode as

$$\hat{W}_{\text{abs}} = \sigma_{\text{abs}}\hat{n}_{km} \tag{2.56}$$

$$\hat{W}_{\text{em}} = \sigma_{\text{em}}\left(\hat{n}_{km}+1\right) \tag{2.57}$$

where $\hat{n}_{km}$ is the photon number operator of the normal mode km and σ_{abs} and σ_{em} are obtained directly from (2.47) and (2.48) and describe the absorption and emission strengths in the media.

For sufficiently small time periods dt the probabilities of emitting or absorbing a single photon are $\hat{p}_{n\rightarrow n-1} = \sigma_{\text{abs}}\hat{n}_{km}dt$ and $\hat{p}_{n\rightarrow n+1} = \sigma_{\text{em}}\hat{n}_{km}dt$ and the probability of emitting or absorbing more than one photon is negligible. For longer time periods the possibility of absorbing or emitting more than one photon must be accounted for. The operator measuring the probability of observing j photons during interval $[t, t+T]$ is

given by [16, 27]

$$\hat{P}_j\left(t, t+T\right) = \hat{O}\frac{\hat{M}^j}{j!}e^{\hat{M}} \tag{2.58}$$

where $\hat{O}$ is the normal ordering operator that arranges the creation operators $\hat{a}^\dagger$ to the left of the annihilation operators $\hat{a}$ and the operator

$$\hat{M} = \int_t^{t+T} \hat{W}_{\rm abs} - \hat{W}_{\rm em} dt = \left(\sigma_{\rm abs} - \sigma_{\rm em}\right)\hat{n}_{km}T \tag{2.59}$$

gives the number of electron - hole pairs created in the interval T. Evaluation of the integral in (2.59) assumes that the detection conditions remain unchanged.

For an ideal detector in which the generated electrons and holes are swiftly swept away from the active region, the emission strength can be approximated as $\sigma_{\rm em} = 0$ and then $\hat{M} = \sigma_{\rm abs}T\hat{n}_{km}$. For a coherent state $|\alpha_{km}>$ the probability of measuring j photons becomes

$$\begin{aligned} P_j =< \alpha_{km}|\hat{P}_j|\alpha_{km} > &= < \alpha_{km}|\hat{O}\frac{\left(\sigma_{\rm abs}T\hat{a}^\dagger_{km}\hat{a}_{km}\right)^j}{j!}e^{\sigma_{\rm abs}T\hat{a}^\dagger_{km}\hat{a}_{km}}|\alpha_{km}> \\ &= \frac{\left(\sigma_{\rm abs}T\left|\alpha_{km}\right|^2\right)^j}{j!}e^{\sigma_{\rm abs}T|\alpha_{km}|^2} \end{aligned} \tag{2.60}$$

which is the Poisson probability distribution. The SNR of a coherent state is given by

$$SNR_{\rm coherent} = \sigma_{\rm abs}T\left|\alpha_{km}\right|^2 = \sigma_{\rm abs}T\overline{n}_{km} \tag{2.61}$$

where $\overline{n}_{km}$ is the average number of photons in the state $|\alpha_{km}>$.

For a large photon reservoir represented by the state $|\Psi >= \sum_n p_n|n_{km}>$ the resulting probability distribution is [16]

$$P_j =< \Psi|\hat{P}_j|\Psi >= \sum_{n=j}^{\infty} p_n \left(\begin{array}{c} n \\ j \end{array}\right)\left(\sigma_{\rm abs}T\right)^j\left(1-\sigma_{\rm abs}T\right)^{n-j}. \tag{2.62}$$

The derivation of these probability distributions doesn't account for the possible change in the photon state as a result of the detection (absorption). Hence the results generally become inaccurate when the detection probability, or quantum efficiency, $\sigma_{\rm abs}T$ approaches unity. More accurate treatments of the measuring process can be found for example in references [28–31].

The probability distribution of chaotic light obtained from (2.62) by using (2.45) has the same form as the original chaotic distribution [16]

$$P_j = \frac{(\sigma_{\text{abs}} T\overline{n})^j}{(1+\sigma_{\text{abs}} T\overline{n})^{1+j}} \tag{2.63}$$

and the SNR of the chaotic state is

$$SNR_{\text{chaotic}} = \frac{\sigma_{\text{abs}} T\overline{n}}{1+\sigma_{\text{abs}} T\overline{n}} \leq 1. \tag{2.64}$$

For long sampling times T the probability distribution for chaotic light is not equal to Eq. (2.63) but approaches again the Poisson distribution (2.60) because of the assumption that $\sigma_{\text{abs}} T \ll 1$ in (2.62) [16]. To achieve high SNR, transfering optical signals should be done using coherent light. If chaotic light is used, the quantum efficiency of the detection should approach unity, ie the sampling time T should be long, to reduce the amount of noise.

Another means to measure an optical signal is by homodyne detectors, where, in addition to a semiconductor detector a beam splitter and a local oscillator are used [23]. The response of a heterodyne detector is proportional to the expectation value of the quadrature operators (2.38)-(2.39), instead of the photon count as in plain semiconductor devices.

3 Components of optical networks

3.1 Semiconductor lasers

Semiconductor lasers are the most important light sources in telecommunications. They are compact, their spectrum is narrow, their wavelength compatible with the transmission windows of optical fibers and they can be operated by electric current. The semiconductor lasers can be classified by the structure of their active region into bulk, quantum well, quantum wire, quantum dot or quantum cascade lasers. Of these, quantum well lasers dominate the market, because their power consumption, processing and other properties make an optimal cost-effective combination of today's technology.

Basically lasers are simple devices: they are forward biased diodes made of a direct bandgap semiconductor and enclosed in an optical cavity (Fig.3.1). In the active region of the diode electrons and holes are simultaneously electrically injected in the conduction and valence bands, respectively. As a result of the recombination of the carriers, photons are emitted by spontaneous and stimulated emission [see Eqs. (2.47)-(2.48)] in the optical modes allowed by the optical cavity.

In the current optical networks the transmitter of choice is usually a quantum well laser (QWL) built in the quaternary $Ga_xAs_yIn_{1-x}P_{1-y}$/InP material system and operating close to the loss minimum of optical fibers (1.55 μm) [32]. In direct modulation standard QWLs exhibit large fluctuations in the optical frequency, ie they chirp. Therefore the transmitters are operated in the CW mode and costly external modulators based on the Pockels effect are used to electrically modulate the signal amplitude.

3.1.1 Laser cavities

The cavity of a semiconductor laser is usually composed of a short waveguide with reflective facet surfaces at both ends. The transverse resonator modes of the cavity can be transverse electric (TE), transverse magnetic (TM) or hybrid modes, depending on the waveguide geometry [19]. The TE (TM) polarization in a planar waveguide is characterized by the electric (magnetic) field in plane of the waveguide and perpendicular to the

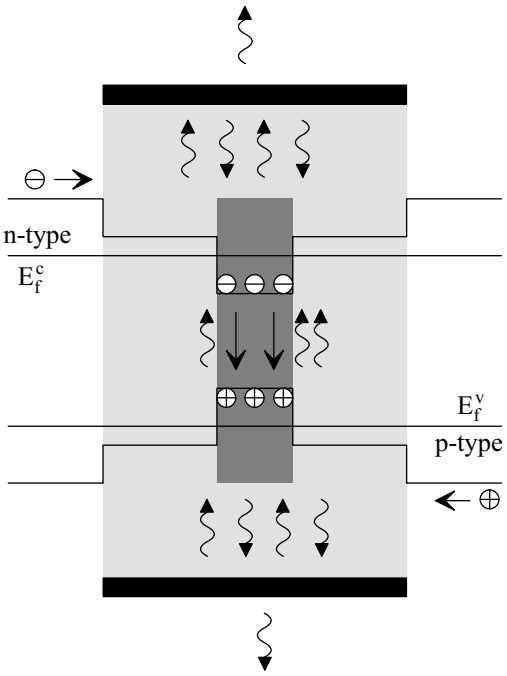

Figure 3.1: Basic operation principle and the schematic structure of double heterostructure semiconductor lasers. Electrical injection in a p-n double heterojunction diode creates a local population inversion in the active region (dark gray). Photons are guided in the waveguide structure formed by the heterojunction interfaces (light gray) and amplified by stimulated emission in the active region. The optical cavity formed by the mirrors or the cleaved semiconductor edge – air interfaces (black) is an optical resonator where optical modes with suitable wavelengths are allowed. The modes that have the highest gain are favored over other modes and have high power and large photon population.

direction of propagation, while the magnetic (electric) field is perpendicular to the electric (magnetic) field and may have a small component in the direction of propagation. In the hybrid modes both the electric and magnetic fields have small components in direction of propagation. Generally, the fewer modes the cavity supports in the region of the positive gain spectrum, the better.

The reflection coefficient R of a conventional symmetrical Fabry-Perot (FP) resonator as a function of the wavelength λ_0 (in vacuum) is [19]

$$R(\lambda_0) = \frac{4R_0 \sin^2 \delta(\lambda_0)}{(1-R_0)^2 + 4R_0 \sin^2 \delta(\lambda_0)} \tag{3.1}$$

where R_0 is the reflection coefficient of the reflecting interface and $\delta(\lambda_0) = 2\pi n_r L/\lambda_0$

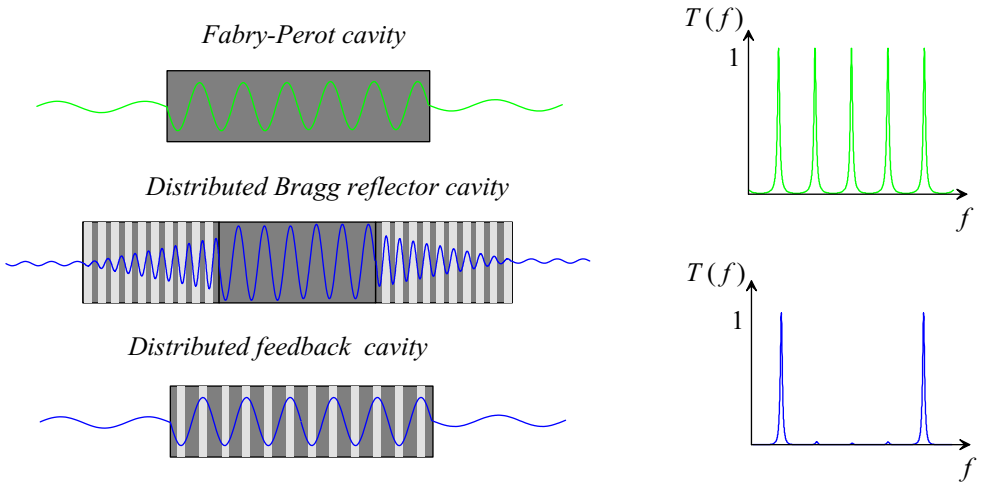

Figure 3.2: Frequency selective resonator structures. In a Fabry-Perot resonator of length L the wavelength λ of an optical signal must satisfy $\lambda n = 2L$ (n is an integer) and the resonance frequencies are closely spaced if L is large. In DBR and DFB type resonators the wavelength must additionally satisfy the resonance condition of the DBR or DFB grating and the spacing of the resonance frequencies can be more freely adjusted.

with n_r being the refractive index in the cavity and L the length of the cavity. The propagation constant k_z (assuming that the waveguide is along z-axis) of the FP resonator satisfies to a good approximation the condition $Lk_z = m\pi$, where m is an integer. If the resonator is long (typical length of a conventional laser is $\lesssim 1$ mm), the resonance frequencies of the longitudinal modes are very closely spaced.

To achieve better frequency selectivity and larger frequency separation, one or both of the mirrors of the FP cavity can be replaced by a distributed Bragg reflector (DBR), which provides high reflectivity for selected frequencies. Alternatively the refractive index in the cavity can be modulated by a distributed feedback (DFB) grating. Then the wavelength must additionally meet the resonance condition of the DBR or the DFB grating. The cavity types and their response are sketched in Fig 3.2.

The quality of an optical cavity for a given wavelength is described by the loss of the cavity α which is affected by scattering, material absorption and the cavity mirrors. The main source of cavity loss is usually caused by the transmission through the cavity

facets. In this case, the loss is approximated by

$$\alpha = -\frac{\ln R}{L}$$

where R is the effective reflectivity of the facet and L is the cavity length.

The DBR or DFB grating increases the cost of the laser significantly. In some applications sufficient frequency selectivity can be reached by using a very short laser cavity instead of the gratings. In vertical cavity surface emitting lasers (VCSELs) the cavity is formed in the growth direction of the substrate and the laser emits light through the surface. VCSELs usually have only one longitudinal mode and are easier to process than DBR or DFB lasers with cavity in plane of the substrate, but often several transverse modes are active in VCSELs.

3.1.2 Laser structures

Double heterostructure lasers, like the one shown in Fig. 3.1, are used to spatially confine both light and carriers in order to optimize the photon-electron coupling. When the width of the potential well where the carriers are confined, gets smaller, quantum effects in carrier distribution become significant. In QWLs the well width is of the order of a few tens of nanometers or less. Reducing the size of the active region in two or three dimensions results in quantum wire lasers and quantum dot lasers (QDLs), respectively. The different active material types and their density of states (DOS) are schematically represented in Fig. 3.3.

The quantization of the eigenstates of the carriers modifies the density of states and affect many properties of the active material. It becomes possible to increase the efficiency of a laser because the threshold gain is reached with smaller injection current. The differential gain in reduced dimensionality active materials becomes higher than in bulk lasers. The modulation induced fluctuations in the optical frequency of the laser, ie chirping and the LEF associated whith chirping is affected by the modified DOS as well. The measured LEF for different laser structures typically ranges from about $\alpha_{\text{lef}} \gtrsim 4$ for bulk lasers to $\alpha_{\text{lef}} \gtrsim 1$ for QWLs and $\alpha_{\text{lef}} \gtrsim 0.1$ for QDLs [20, 33–40]. These values naturally depend on the specific operating point and measuring frequency, but they

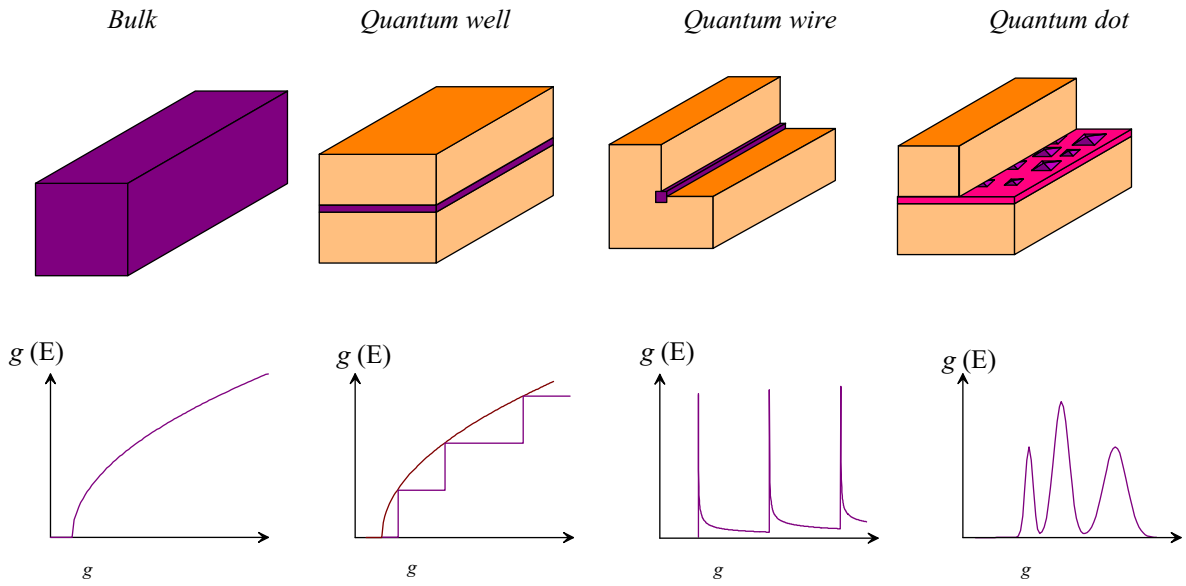

Figure 3.3: Density of states in active materials exhibiting different quantum features. In bulk material the density of states is proportional to $\sqrt{E - E_g}$. In quantum wells the density of states is of the step function form and in quantum wires it is proportional to $1/\sqrt{E - E_g}$. In quantum dots the DOS is basically a delta-function, but because the dot sizes and energies fluctuate from dot to dot, the effective DOS of the dots becomes Gaussian and has a finite width.

indicate a general tendency of achieving lower LEF for reduced dimensionality active materials.

3.1.3 Properties of quantum dot lasers

From the middle of the 1990s, it has become possible to fabricate QDLs operating at room temperature. The active material in these lasers is made of self-organized quantum dots fabricated by the modified Stranski-Krastanov method [41]. The manufacturing of the active material in QDLs is based on growing a thin film (a few monolayers) of a semiconductor material on top of the substrate (for example $In_xGa_{1-x}As$ on GaAs) by molecular beam epitaxy or metal organic vapor phase epitaxy. If the lattice constant of the film is mismatched with that of the substrate, the film breaks when the layer reaches a critical thickness and the newly deposited atoms form numerous small islands and pos-

sibly a monolayer thick wetting layer between them. The quantum dots (QDs) can then be overgrown by a suitable barrier material. These steps can be repeated several times leading to a stack with many QD layers.

The density of states of a single QD is delta function -like and only broadened by the finite lifetimes of the carriers in the dots. The homogeneous lifetime broadening has the Lorentzian form [42]

$$L_L(E) = \frac{\Gamma_\tau/\pi}{(E - E_g - E_0)^2 + \Gamma_\tau^2} \tag{3.2}$$

where $\Gamma_\tau = \hbar/\tau$ and τ is the lifetime of the state, E_g the band gap energy of the QD material and E_0 the quantization energy of the dot. However, due to the self-organized growth of the islands, the DOS of the QD system is also inhomogeneously broadened. The inhomogeneous broadening leads to the QD eigenstate energy distribution that obey the normal distribution [41]

$$L_G(E) = \frac{1}{\sqrt{2\pi\sigma_E^2}} e^{-(E-E_g-E_0)^2/(2\sigma_E)^2} \tag{3.3}$$

$$\sigma_E \approx 2\varsigma E_0. \tag{3.4}$$

The probability L_G that the QD states with transition energy E exist depends on the relative standard deviation ς ($\varsigma \gtrsim 0.1$) of the energy states [43]. The inhomogeneous broadening (typically $\sim 10 - 20$ meV) usually dominates over the homogeneous lifetime broadening (~ 0.1 meV), and the lifetime broadening can be neglected in the eigenstate energy distribution of QDs.

The distinguished density of states of the QDLs offers many potential advantages over other active materials [43–47]. The threshold current density in the QDLs can be significantly lower than in the more conventional QWLs resulting in higher efficiency. The differential gain is higher and the frequency fluctuations caused by the changes in the carrier density can be made smaller.

Formerly it was believed that the relaxation processes of the carriers in the inhomogeneously broadened QDs was severely limited by the so called phonon bottleneck and that the spectral hole burning would make QDLs unpractical [48, 49]. However, more recent studies suggest that the relaxation processes are sufficiently fast for the QDs to reach

thermal quasi-equilibrium with reasonable output powers [50, 51]. This approximation significantly simplifies dynamical modeling of QDLs.

The advantages of using QDLs as directly modulated transmitters depend on the possibility of reducing the chirp and the inhomogeneous broadening. It has often been argued that due to the symmetrical DOS the LEF of QDLs is inherently very close to zero at the lasing frequency [33–35]. However, this may only apply when the inhomogeneous broadening is small compared to the lifetime broadening, which is not the case for self-organized QDs. Even perfectly symmetric DOS does not result in zero LEF at the gain peak for numerous reasons, if the energy spectrum of the dots is inhomogeneously broadened (see Publication I for further details). The effect of tuning the LEFs in QWLs by shifting the lasing wavelength has been generally acknowledged in QWLs for some time [52]. The same method to control the LEF is not only possible in QDLs, but the required shift and the resulting increase in the threshold current are smaller and more easily achievable.

3.1.4 A dynamical laser model: the rate equations

Describing an optical system directly with the quantum mechanical or even the classical equations becomes highly unpractical when the system composes of several separate components. There are several approximations that can be used to simplify the system. One of the most widely adapted methods in modeling the dynamics of optical components are the rate equations, which describe the average carrier density and the average photon densities in different optical modes whose frequencies are widely separated from one another [19].

Rate equations describe the rate of change of the carrier (n_e) or photon (n_L) density of a cavity mode by simple, often linear, approximate laws obtained experimentally or theoretically. For a typical current injected single mode laser, the equations are of the form

$$\frac{dn_e}{dt} = W_{\text{inj}} - cg\left(n_e\right) n_L - W_{\text{nst}} \tag{3.5}$$

$$\frac{dn_L}{dt} = c\left[g\left(n_e\right) - \alpha\right] n_L + W_{\text{sp}} + W_{\text{ext}}. \tag{3.6}$$

The rate of change of the carrier density is divided in three terms. The carrier density is increased by the current injection, given by the term $W_{\text{inj}} = I_{\text{eff}}/eV$, where I_{eff} is the effective injection current and V is the effective volume of optical cavity (or the active region, depending on the normalization). On the other hand, the carrier density is decreased by stimulated emission at the rate $cg(n_e)n_L$ and by the other recombination processes W_{nst}. Often one can well approximate $W_{\text{nst}} \approx n_e/\tau$ where τ is the average lifetime of carriers, excluding the recombination by the stimulated emission process.

The photon density in the cavity changes due to the gain (the combined effect of stimulated emission and absorption) g and the losses of the cavity α. The cavity losses contain the scattering losses α_{sc} and the mirror losses $\alpha_{\text{mirror}} = -\ln R/L$, where R is the mirror reflection coefficient and L the length of the cavity. Additional sources of photons that may increase the photon density are the spontaneous emission into the laser mode W_{sp} and the rate W_{ext} at which photons are injected into the cavity from outside sources.

In phase locked lasers, there is an external coherent optical signal injected to the laser. To account for the phase of the signal, Eq. (3.6) must be modified to describe the complex electric field phasor E_L of the laser instead of the average carrier density [53,54]. The equation describing the optical field then becomes

$$\frac{dE_L}{dt} = \frac{c}{2}\left[g(n_e) - \alpha + i\Delta\omega(n_e)\right]E_L + \frac{c}{2L}E_{\text{ext}}. \tag{3.7}$$

Here $\Delta\omega(n_e) = \alpha_{\text{lef}}\Delta\alpha(n_e)$ is the difference between the frequency of the externally injected field E_{ext} and the resonance frequency of the cavity mode, which depends on the carrier density. The change in the absorption $\Delta\alpha(n_e)$ is calculated with respect to the absorption at which the cavity resonance coincides with the frequency of the external signal E_{ext}.

3.1.5 Small signal modulation properties of lasers

The small signal analysis of a laser is instructive to see what factors in general affect the operating speed of a semiconductor laser. This information is also important in the evaluation of the capabilities of the coherent nonlinear devices to be introduced in this

thesis. The rate equations of a single mode laser in the small signal approximation are

$$\frac{dn_{\delta e}}{dt} = -\left(c\gamma_L n_{L0} + \frac{1}{\tau}\right) n_{\delta e} - c\alpha_L n_{\delta L} + \Delta \tag{3.8}$$

$$\frac{dn_{\delta L}}{dt} = c\gamma_L n_{L0} n_{\delta e} \tag{3.9}$$

where the carrier and photon densities $n_e = n_{e0} + n_{\delta e}$ and $n_L = n_{L0} + n_{\delta L}$ have been divided in constant parts n_{e0} and n_{L0} and a small deviation from the constant values, $n_{\delta e}$ and $n_{\delta L}$. The term $\gamma_L = dg_L\left(n_e\right)/dn_e|_{n_e=n_{e0}}$ denotes the differential gain of the laser and Δ is the change in the injection. Making a Laplace transformation for the equations and solving for the carrier density deviation gives

$$\mathcal{L}\left\{n_{\delta e}\right\} = \frac{-s\mathcal{L}\left\{\Delta\right\}}{c^2\gamma_L n_{L0}\alpha_L + s^2 + s\left(1/\tau + c\gamma_L n_{L0}\right)} \tag{3.10}$$

$$\mathcal{L}\left\{n_{\delta L}\right\} = c\gamma_L n_{L0}\frac{\mathcal{L}\left\{n_{\delta e}\right\}}{s}. \tag{3.11}$$

The solutions of (3.10) in time domain for a step function input, $\mathcal{L}\left\{\Delta\right\} = 1/s$, are easily obtained using partial fraction decomposition in the form

$$n_{\delta e}\left(t\right) = \frac{1}{s_1 - s_2}\left(e^{s_1 t} - e^{s_2 t}\right) \tag{3.12}$$

where $s_{1,2}$ are the poles of Eq. (3.10). The characteristics of the solution are then easily deduced from location of the poles. If the poles have an imaginary part, the solutions are oscillatory (relaxation oscillations occur). If they are real, the solution moves to its new steady state value monotonously. The discriminant of the denominator of (3.10) is

$$D = \left(1/\tau + c\gamma_L n_{L0}\right)^2 - 4c^2\gamma_L n_{L0}\alpha_L. \tag{3.13}$$

Real solutions are obtained if $D \geq 0$, ie

$$\alpha_L \leq \frac{\left(1/\tau + c\gamma_L n_{L0}\right)^2}{4c^2\gamma_L n_{L0}} \approx \frac{\gamma_L n_{L0}}{4} \tag{3.14}$$

where the latter approximation assumes that the term $c\gamma_L n_{L0} \gg 1/\tau$. In single mode lasers the relaxation oscillations therefore disappear if the laser is biased so that the (steady state) photon density - differential gain product $\gamma_L n_{L0}$ is sufficiently large. The

decay time of the perturbation is obtained from the poles s_1 and s_2 of (3.10) according to (3.12). The poles are given by

$$s_1 = \frac{-(1/\tau + c\gamma_L n_{L0}) - \sqrt{D}}{2} \tag{3.15}$$

$$s_2 = \frac{-(1/\tau + c\gamma_L n_{L0}) + \sqrt{D}}{2}. \tag{3.16}$$

The outcome of the simple timescale derivation above shows that the operating speed of current injected lasers is limited by the carrier lifetime at low output powers. At higher powers the large number of photons in the cavity begins to dominate and the operating speed begins to grow ($s_1 \rightarrow -\infty$, $s_2 \rightarrow -c\alpha_L$ as $n_{L0} \rightarrow \infty$) . In the on-off amplitude modulation the small signal analysis does not give accurate results, although it makes it easier to appreciate the slow response caused by the vanishing of the photon population in the off state. In practise the direct current modulation frequency of the lasers is limited to a few tens of GHz [39, 55].

The results calculated for a laser with one laser mode and one signal mode differ from the simple results derived here by an additional time constant $c(\alpha_S - g_S)/20$, where α_S and g_S are the losses and the gain of the signal mode (see Publication III). Although small signal approximation can not accurately describe operation in large signal conditions, they give an estimate on the operating speed obtainable by a laser construction that always has a nonzero photon population in the laser mode.

3.1.6 Photon statistics of laser generated light

Photon statistics of the light generated by lasers can be evaluated by using rate equations written for the weight coefficients $p_n(t)$ of the state $|\Psi> = \sum_n p_n(t)\,|n_{km}>$ [16]. The outcome for a laser that is above the threshold is

$$P_n = \frac{(\beta + \overline{n}_{km})^{\beta+n}}{(\beta+n)!} e^{(-\beta-\overline{n}_{km})} \tag{3.17}$$

where $\overline{n}_{km}$ is the average number of photons in the mode and β is a parameter describing the strength of spontaneous emission with respect to the pumping rate (β decreases as pumping becomes stronger). With high pumping rates the distribution (3.17) approaches

Poisson distribution and therefore the light emitted by a good quality laser is approximately coherent. If the laser operates below the laser threshold the photon distribution becomes chaotic. Note that the coherence of lasers is just a result of the process where the delicate interaction between the photons, the active medium and the cavity results in a photon distribution that corresponds to the distribution of coherent light.

The signal to noise ratio of a signal measured by a photodetector and generated by a laser can be calculated using (3.17) and (2.54). When the relative power of spontaneous emission becomes negligible far above the laser threshold ($\beta = 0$), the SNR approaches the value obtained for coherent light (2.61) and the noise level is reduced when the output power of the laser is increased. Below and very close to the threshold the SNR approaches (2.64) for short measuring times.

Another measure of the laser signal quality is the linewidth of the laser. The laser linewidth can be approximated semiclassically starting from the properties of spontaneous emission and stimulated emission and their relative powers in the laser [56]. If the cavity mode has $\overline{n}_{km}$ photons on average, there is one spontaneous emission process for each $\overline{n}_{km} - 1 \approx \overline{n}_{km}$ stimulated emission processes. Since stimulated emission processes tend to conserve the coherent statistics and spontaneously emitted photons tend to destroy coherence, the situation can be described by a coherent electric field phasor with $\overline{n}_{km}$ photons on average being perturbed by one photon with a random phase. A single spontaneously emitted photon can then cause a phase shift of $\Delta\phi \approx 1/\sqrt{\overline{n}_{km}}$ radians. The random walk process changes the electric field phasor at a rate $(\Delta\phi)^2 / \tau_{\text{cav}} = (\tau_{\text{cav}}\overline{n}_{km})^{-1}$ where τ_{cav} is the cavity lifetime for the photons. The laser linewidth then becomes [56]

$$\Delta f \approx \frac{1}{2\pi\overline{n}_{km}\tau_{\text{cav}}}. \tag{3.18}$$

Writing the result with the average photon count replaced with the optical power P and accounting for the linewidth enhancement factor of semiconductors gives

$$\Delta f \approx \frac{\hbar\omega\left(1+\alpha_{\text{lef}}\right)^2}{2\pi\tau_{\text{cav}}^2 P} \tag{3.19}$$

as the linewidth of the laser.

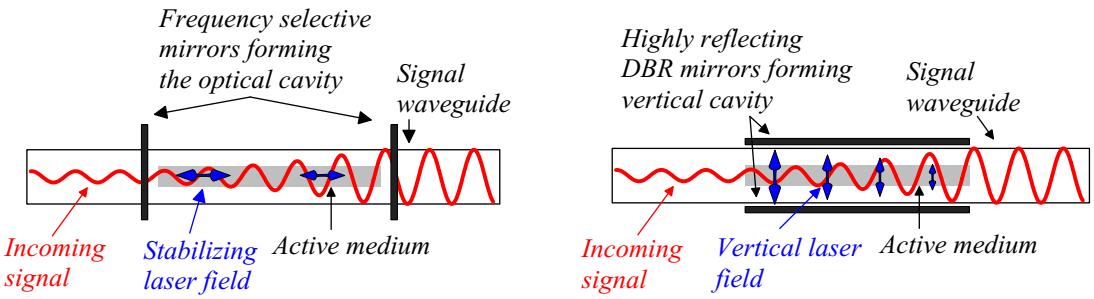

Figure 3.4: Gain clamped semiconductor optical amplifiers are lasers which allow the amplified signal(s) to propagate through an optical cavity with an active laser mode. In the conventional traveling wave GCSOA the laser cavity, formed by two frequency selective mirrors, is parallel with the signal waveguide (a). In the so called linear optical amplifiers (LOA) the laser field is perpendicular to the signal waveguide (b). When the signal is amplified it takes power from the laser mode. In LOA this results in pronounced spatial variation of the laser field.

3.2 Gain clamped optical amplifiers

Impurity doped fiber optical amplifiers are commonly used in the optical networks. Their largest drawbacks are their bulky size, the requirement of optical pumping and the gradual saturation as the input power increases. Alternatives for the fiber amplifiers ranging from Raman fiber amplifiers to several kinds of semiconductor devices have been proposed [19, 57,58]. The most interesting alternatives, in the context of this thesis, are the gain clamped semiconductor optical amplifiers (GCSOAs). These amplifiers are operated directly with current and their response is more linear than that of conventional fiber optical amplifiers or semiconductor optical amplifiers (SOAs). Furthermore, they are used in the optical flip-flops described later in this thesis.

The operation of the GCSOAs is based on amplifying the signal by stimulated emission in the presence of an additional laser field (Fig. 3.4). The laser field is confined in a cavity that is parallel to the direction of signal propagation (conventional GCSOA) or perpendicular to it (linear optical amplifier (LOA)). In GCSOAs the overall gain of the laser mode needs to be higher than the gain of the signal mode. This can be achieved either by frequency selective mirrors or by frequency selective gain in conventional GCSOAs. In LOA the mirrors need not have any frequency selectivity because

different mirrors are used for the signal and laser modes. The amplifiers where the signal propagates through the amplifier without reflections are further categorized as traveling wave amplifiers (TWAs) while the amplifiers where the signal is filtered by an optical cavity are of the Fabry-Perot amplifier (FPA) type.

A generalized position dependent rate equation model of the form

$$\frac{\partial n_e(x,t)}{\partial t} = W_{\text{inj}} - cg_L n_L(x,t) - c\sum_{i,\kappa} g_i s_{i,\kappa}(x,t) - \frac{n_e(x,t)}{\tau} \quad (3.20)$$

$$\frac{\partial n_L(x,t)}{\partial t} = c(g_L - \alpha_L) n_L(x,t) \quad (3.21)$$

$$\frac{\partial s_{i,\kappa}(x,t)}{\partial t} = -\kappa c \frac{\partial s_{i,\kappa}(x,t)}{\partial x} + cg_i s_{i,\kappa}(x,t) \quad (3.22)$$

can be used to describe either one of the amplifier types when boundary conditions that suitably account for the reflections at the cavity ends are used. Here $n_L(x,t)$ is the photon density in the vertical laser field (applicable only for LOA), $s_{i,\kappa}(x,t)$ the photon density of the signal mode i propagating in the $+x$ $(\kappa = 1)$ or $-x$ $(\kappa = -1)$ direction. The gain of the GCSOAs is basically determined by the threshold value (α_L in case of LOA) that is required for laser operation. The gain stays approximately constant while the laser is above the threshold and only the optical power of the laser mode changes when the signal is amplified. This process minimizes changes in the amplification and carrier density and the amplifier is very tolerant to variations in the input signal.

In Publication II the differences of the TWAs of the SOA, GCSOA and LOA types are studied. The results verify that the gain of both GCSOA types, the conventional GCSOA and the LOA, are quite independent of the input signal power. An approximation where the rate equations are averaged over the length of the amplifier is also possible with good accuracy [59]. This approximation applies especially well for the FPAs and is adapted in the other publications of this thesis.

3.2.1 Photon statistics of optical amplifiers

The quantum mechanical approach to the photon statistics of an optical amplifier is based on writing the rate equations for the probability distribution $p_n(t)$ of the state $\sum_n p_n(t) |n_{km}>$ in the normal mode km in a two level picture and solving the time

evolution of the probability distribution. This approach leads to the Kolmogorov equations that describe the evolution of the probabilities $p_n(t)$ [60–62]. Despite the apparent difference in the phenomenology at the first sight, the equations are formally similar to the equations describing the biological birth-death-immigration processes [63]. This makes the problem conceptually straightforward and easy to simulate stochastically.

Basically, a group of photons enters an amplifier. As they propagate along the amplifier there is a chance per unit time (distance) that any of the photons get absorbed (death), generate a new photon by stimulated emission (birth) or that a spontaneously emitted photon is created (immigration).

Closed form solutions to the probability distributions at the output of a traveling wave amplifier are readily available in the form of probability generating functions (PGFs), from which the mean and higher moments are easily obtained [64]. The probability generating function at the input of an amplifier is defined by

$$F_0(\zeta) = \sum_n p_{0,n}\zeta^n \tag{3.23}$$

where $p_{0,n}$ is the probability of there being n photons at the input at time $t = 0$ and ζ is a real parameter. The PGF at the output becomes

$$F(\zeta, t) = F_0(Z(\zeta, t; 0))\, e^{\int_0^t [Z(\zeta,t;\tau)-1]\nu(\tau)d\tau} \tag{3.24}$$

where

$$Z(\zeta, t; \tau) = 1 + \frac{(\zeta - 1)\, h(\tau)}{h(t) - [\zeta - 1]\left[\int_0^t h(u)\,\lambda(u)\,du - \int_0^\tau h(u)\,\lambda(u)\,du\right]} \tag{3.25}$$

$$h(u) = e^{\int_0^u \mu(t)-\lambda(t)du} \tag{3.26}$$

and $\lambda(t)$ is the birth rate, $\mu(t)$ is the death rate and $\nu(t)$ is the immigration rate.

An important special case of the output probability generating function (3.24) is the probability density in the case of coherent light at the input of a TWA. The probability density is of the noncentral-negative-binomial (NNB) form,

$$p_n = \frac{\overline{n_{\text{amp}}}^n}{(1 + \overline{n_{\text{amp}}})^{n+M}} e^{-G\overline{n_s}/(1+\overline{n_{\text{amp}}})} L_n^{M-1}\left[-\frac{G\overline{n_s}}{\overline{n_{\text{amp}}}\,(1 + \overline{n_{\text{amp}}})}\right] \tag{3.27}$$

where $\overline{n_{\mathrm{amp}}} = G(L)\int_0^L \gamma_{\mathrm{st}}(z)/G(z)\,dz$, γ_{st} is the stimulated emission rate, $G(L)$ is the amplification of the amplifier from 0 to L, $\overline{n_s}$ is the mean photon number at the input, $M = M'T/t_c$, M' is the number of modes available for spontaneous emission, T is the measuring time, t_c is the coherence time and $L_n^{(M-1)}$ is the Laguerre polynomial.

The mean and variance of the distribution (3.27) are [65–67]

$$\overline{n} = G\overline{n_s} + M\overline{n_{\mathrm{amp}}} \tag{3.28}$$

$$Var\{n\} = G\overline{n_s} + 2G\overline{n_s}\,\overline{n_{\mathrm{amp}}} + M\overline{n_{\mathrm{amp}}}\,(1+\overline{n_{\mathrm{amp}}})\,. \tag{3.29}$$

The components of the variance in the output photon distribution are the amplified noise of the input signal (first term), the noise added by the random amplification process (second term) and the spontaneously emitted photons that are also amplified (last term). From these results the fundamental limitation of optical amplifiers, the lowest achievable noise factor of ~ 2, becomes apparent. Even if the amplified spontaneous emission is negligible (last term ~ 0), the noise associated with the fluctuations in the amplification is significant. For constant gain along the amplifier $\langle n_{\mathrm{amp}}\rangle = (G-1)\,\gamma_{\mathrm{st}}/(\gamma_{\mathrm{st}}-\gamma_{\mathrm{abs}}) \geq G-1$ with γ_{abs} being the absorption rate. The noise factor for $G \gg 1$ then becomes

$$NF = \frac{G + 2G(G-1)}{G^2} \to 2. \tag{3.30}$$

Other types of optical amplifiers which exploit the quadrature states of light and use complicated setups, may, however, provide lower noise figures in specific circumstances [68].

3.3 Nonlinear effects

In the classical theory the light - matter interaction is accounted for by the material parameters ε and μ that are functions of the electric field $\mathbf{E}$. Usually the variations in the permeability μ are small and neglected. The relative permittivity can be expanded in powers of the electric field $\mathbf{E}$:

$$\varepsilon_r(\mathbf{E}) = 1 + \sum_{i=0}^{\infty} \chi^{(i)}\mathbf{E}^i, \tag{3.31}$$

where $\chi^{(i)}$ are the expansion coefficients of the susceptibility. The best known nonlinear effects that are used in nonlinear optical components are the Pockel's effect ($j = 1$) and the Kerr effect ($j = 2$).

Pockel's effect is found in crystals lacking inversion symmetry, such as lithium niobate ($LiNbO_3$, $\chi^{(1)} \sim 10^{-11}$ m/V) or gallium arsenide ($\chi^{(2)} \sim 10^{-13}$ m/V) [32]. The effect is predominantly used in electro-optic modulators [69]. The Kerr effect is a second order effect, in which the material permittivity changes in proportion to the intensity ($\sim \mathbf{E}^2$) of the light. All materials exhibit Kerr effect, although in most cases it's extremely weak. Kerr effect is also responsible for self focusing and self phase-modulation and it is an important factor in soliton formation. The nonlinearity of matter is the key element in many prototypes or theoretical descriptions of nonlinear optical devices [6, 70–72].

3.4 Nonlinear optical components

The most important device types for the next generation optical networks are the optical isolators, switches, regenerators, memories and logic gates that are suitable for integration. Many variations of these devices have been demonstrated over the years with different operating principles. Some examples of these operating principles and references to the devices are given below.

Discrete optical isolators are based on the Faraday rotation which has not been successfully demonstrated in integrated form. Alternative techniques for the integrated environment are for example using nonlinear asymmetric structures or inducing a nonresiprocal absorption in an amplifying waveguide by introducing a layer of ferromagnetic metal close to the waveguide [71, 73, 74]. These techniques are suitable for integration in principle, but their performance is not sufficient to date.

All-optical switching is most often based on changing the optical length of an interferometer arm or the resonance condition of a resonator. Common methods to achieve this are the Kerr effect or the use of optical components like the SOA that saturate with optical power [75–77].

In many cases optical logic gates, threshold circuits and memories are strongly in-

tertwined and the same technology can be used to realize all of the devices with only minor modifications. Optical regenerators have been realized using the saturation effects in optical amplifiers, mode hopping in side-mode injection-locked lasers and phase modulation in interferometers [78–83]. Optical logic gates exploit the same saturation and phase modulation effects as regenerators [84–89]. In addition logic gates based on polarization rotation, periodic nonlinear structures and wavelength converters have been reported [90–92].

In principle optical flip-flop circuits can be trivially realized by arranging two optical logic gates in a suitable feedback configuration, just like in electronics. However, many, if not most, flip-flop circuits are based on bistable lasers or on the bistability of two coupled lasers. First bistable laser structures were based on the coexistence of saturable absorbers and active material with gain in the same laser cavity [93–96]. Later realizations of optical flip-flops use separate lasers with feedback between them [97–99]. All of these flip-flop configurations involve switching on and of at least one laser field when the flip-flop changes state.

4 Coupled systems of coherent gain clamped laser amplifiers

In this chapter a new nonlinearity based on using gain clamped amplifiers together with interferometers is introduced. The nonlinearity has potentially much faster response than the nonlinearities previously utilized in implementing nonlinear optical devices. The nonlinearity is suitable for creating for example optical flip-flop circuits, regenerators and logic gates. The advantage of the nonlinearity is that it is present above the laser threshold, in contrast to the previously introduced nonlinearities of bistable lasers, coupled GCSOAs, microring lasers etc, in which the nonlinearity is strongest at the laser threshold.

4.1 Fast nonlinearity by interference

Interference of coherent optical signals is inherently a very fast process. The complex electric field phasor E_{out} at the output of a balanced two arm interferometer [Fig. 4.1(a)] is given by [25]

$$E_{\text{out}} = \frac{1}{\sqrt{2}}\left(E_{\text{in}} + E_b\right) \tag{4.1}$$

where E_{in} and E_b are the electric field phasors at the two inputs of the interferometer. Input E_b is later referred to as the bias signal and E_{in} as the input signal. The corresponding optical output power $P_{\text{out}}\left(E_{\text{out}}\right)$ of the interferometer as a function of the input powers $P_{\text{in}}\left(E_{\text{in}}\right)$ and $P_b\left(E_b\right)$ and the phase difference ϕ between E_{in} and E_b is

$$P_{\text{out}} = \frac{1}{2}\left[P_{\text{in}} + P_b + 2\sqrt{P_{\text{in}}P_b}\cos\phi\right]. \tag{4.2}$$

Scaling (4.2) with the variables $P'_{\text{out}} = P_{\text{out}}/P_b$ and $P'_{\text{in}} = P_{\text{in}}/P_b$ corresponds to amplifying or attenuating the input and output signals. The scaled output power is

$$P'_{\text{out}} = \frac{1}{2}\left[P'_{\text{in}} + 1 + 2\sqrt{P'_{\text{in}}}\cos\phi\right] \tag{4.3}$$

which reveals that the response of any two interferometers with constant input bias fields E_b^1 and $E_b^2 \neq E_b^1$ is identical if the input and output signals of the interferometers are scaled by $1/E_b^1$ and $1/E_b^2$, respectively.

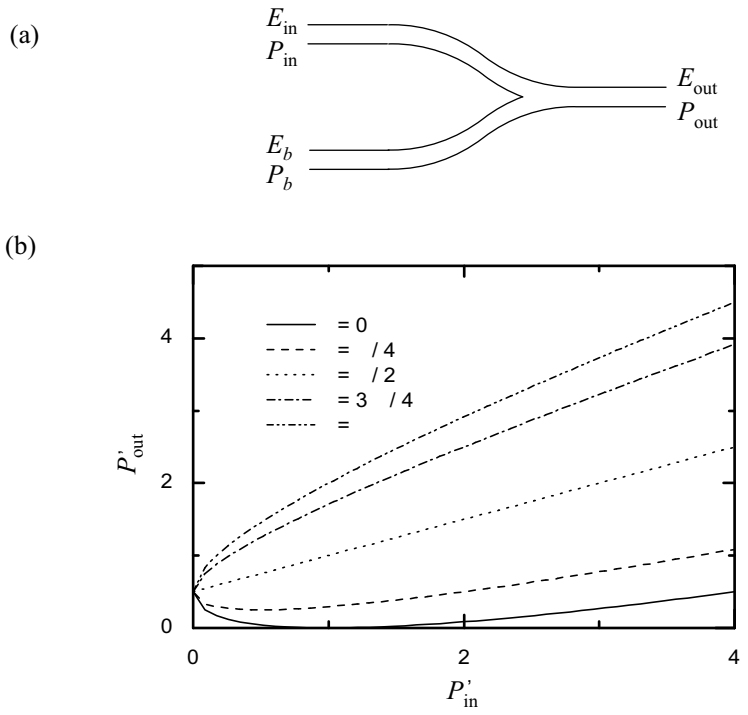

Figure 4.1: (a) A two arm interferometer and (b) the output power (4.3) of the interferometer for various phase differences between the input signals. The strongest nonlinearity is obtained for the value $\phi = \pi$.

Equation (4.1) shows that interference is a linear process in terms of the electric field. In terms of the optical power [Eq. (4.2)], however, the transfer function is nonlinear if $\phi \neq \pm\pi/2$. The strongest nonlinearity is obtained for $\phi = \pi$ as shown in Fig. 4.1(b).

Even though the output optical power of an arbitrary interferometer structure is a nonlinear function of the input power for $\phi \neq \pm\pi/2$, the output electric field is a linear function of the input fields. However, combining the nonlinearity (in terms of optical power) of the interferometers with the nonlinearity (in terms of electric field) of some other structure allows one to create functions that are nonlinear both in terms of the electric field and the optical power.

In this thesis the electric field nonlinearity to be combined with the nonlinearity of the interferometers is obtained by utilizing GCSOAs. The output power P_{out} of a GCSOA at the laser mode wavelength λ_L of the GCSOA is a function of the input power P_{in} at the

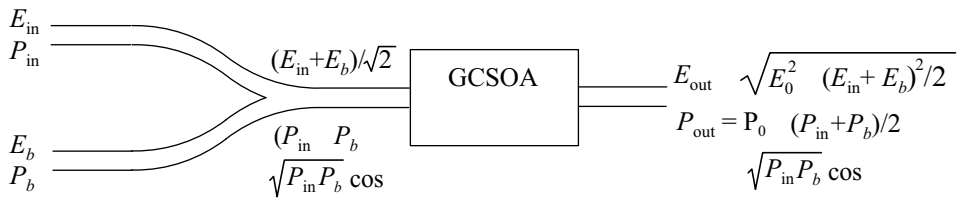

Figure 4.2: Combining an interferometer with a GCSOA allows creating nonlinear functions of the form (4.6). In a GCSOA the cavity mode with wavelength λ_L is above the laser threshold and active even if no input signals are present. In the signal mode with wavelength λ_s there is optical power only when an input signal is present. The signals at different locations are marked in the picture by using both the electric field and optical power and with $C = 1$. The expressions to the left of the GCSOA correspond to the power and electric field of the signal mode λ_s of the GCSOA. To the right they refer to the laser mode λ_L of the GCSOA. The response time is limited by the modulation properties of the amplifier, but can be very high if the operating point and the properties of the amplifier are optimized.

signal mode wavelength λ_s ($\lambda_s \neq \lambda_L$). Above the laser threshold the output power P_{out} can be approximated as

$$P_{\text{out}} = P_0 - CP_{\text{in}} \tag{4.4}$$

where P_0 is the output power of the laser mode when the power of all other modes is ~ 0 and C is a factor of proportionality that describes the amplification of the signal. For $C < 0$ the signal is absorbed and for $C > 0$ it is amplified. In terms of the electric field the output of the GCSOA is given by

$$E_{\text{out}} = \sqrt{E_0^2 - CE_{\text{in}}^2} \tag{4.5}$$

where E_0 is the electric field of the mode λ_L when there is no input electric field, ie $E_{\text{in}} = 0$.

With an interferometer and a phase locked GCSOA (Fig. 4.2) it becomes possible to generate functions of the form (all equations are equivalent)

$$P_{\text{out}} = P_0 - \frac{1}{2}C\left(\sqrt{P_b} - \sqrt{P_{\text{in}}}\right)^2 \tag{4.6}$$

$$P'_{\text{out}} = 1 - \frac{1}{2}C\left(\sqrt{P'_b} - \sqrt{P'_{\text{in}}}\right)^2 \tag{4.7}$$

$$E_{\text{out}} = \sqrt{E_0^2 - \frac{1}{2}C\left(E_b + E_{\text{in}}\right)^2} \tag{4.8}$$

when the phase difference of the signals entering the interferometer is set to $\phi = \pi$ in Eqs. (4.2) and (4.3). The primed variables are obtained by scaling with $1/P_0$. Functions (4.6)-(4.8) are nonlinear *both* in terms of the electric field *and* the optical power, in contrast to (4.2) and (4.4). Now the functions (4.7) with different ratios $P_b' = P_b/P_0$ can no longer be reproduced from one another by scaling the input and output of the interferometer – GCSOA combination, like in the case of a simple interferometer (4.3). In principle the interferometer – GCSOA structures can be chained or used as a basis to generate other functions, like the regenerator function of Publication III. In this thesis it is always assumed $C > 0$, but constructing flip-flop configurations where $C < 0$ is possible as well. This could actually be an important simplification for processing the devices, because then the active region could have negative gain at the signal frequency.

Note that the optical fields in the input of the interferometers are coherent and have a constant phase difference of $\phi = \pi$. The requirement of constant phase difference $\phi = \pi$ can be satisfied by locking the phase of the input signal E_{in} to the phase of the constant bias signal E_b. The most straightforward way to do that in the components modeled in this thesis is to phase lock the laser field of the GCSOA.

The major advantage of the combined nonlinearity of interferometry and of GCSOAs is the potential for high speed operation. In most other nonlinear devices involving lasers, the nonlinearity originates from the laser threshold when setting on and off the lasers. Operating the lasers on both sides of the laser threshold limits the speed of the device.

4.2 Coherent optical Flip-Flops

The nonlinearity achieved by using interferometers and GCSOAs in the previous section provides a new mechanism to create nonlinear feedback between two GCSOAs. The nonlinear feedback can be used to create an optical flip-flop memory, the coherent optical flip-flop (COFF), based on a bistable configuration of two GCSOAs.

The laser modes of the two GCSOAs, L_1 and L_2 are denoted by λ_1 and λ_2 ($\lambda_1 \neq \lambda_2$), respectively. The signal modes occur correspondingly at λ_2 and λ_1. Additionally the GCSOAs support a third mode λ_3 that allows setting and resetting the COFF. The

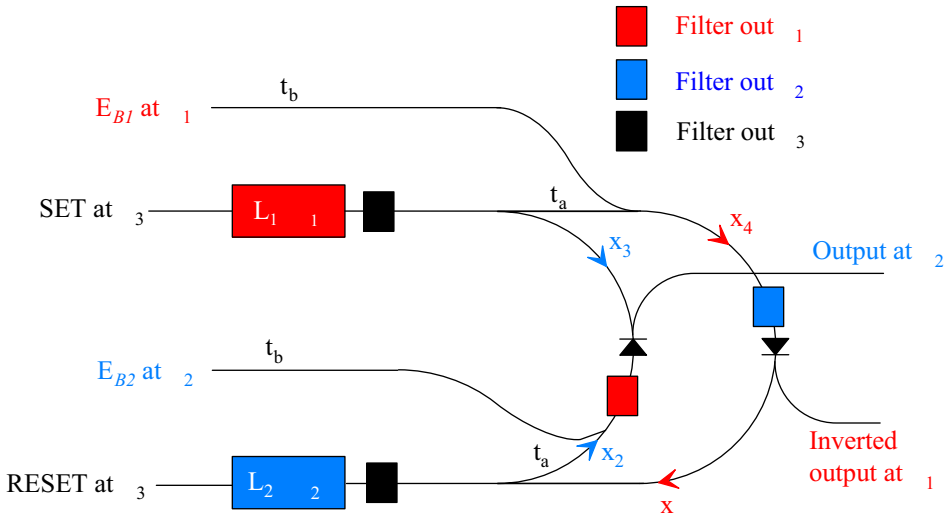

Figure 4.3: A foherent optical flip-flop (COFF) with two bistable states can be created if biased interferometers are used in the feedback channel between two phase locked GCSOAs with different laser mode frequencies. The COFF may be constructed using the two GCSOAs, two optical isolators and optical filters. The set- and reset-operations of the flip-flop are done by sending light pulses to the respective input ports, and the output (inverted output) of the COFF can be read from the respective output ports. The laser modes of the GCSOAs L_1 and L_2 are λ_1 and λ_2, respectively.

GCSOAs are arranged so that λ_1 (λ_2) is injected into L_2 (L_1) as the feedback signal after making it interfere with a suitable constant bias signal t_b. The bistability of the COFF is based on a feedback scheme whose speed is limited by the response time of the GCSOA. The difference to previous bistable laser systems is that the laser mode maintains a large photon population at all times, which allows fast operation [(3.15)-(3.16)].

In the simplest form, if optical isolators are available, the COFF is formed of two phase locked GCSOA, two interferometers, two optical isolators and two coherent light sources used as the sources of the bias signals and the phase locking (Fig. 4.3). The feedback equation of the system is derived in the following by tracing the feedback signal x through the waveguides, interferometers and the GCSOAs. In the derivation the cavity response is omitted for simplicity, $C = 1$, parameter t_a describes the strength of the coupling between the GCSOAs, t_b the strength of the bias signal and parameters E_{0L1} and E_{0L2} the maximum electric field of the GCSOA when no input is present.

To generate the feedback equation, the feedback signal x is first followed into GCSOA L_2 where it interacts with the laser mode λ_2 resulting in $x_1 = \sqrt{E_{0L2}^2 - |x|^2}$. The output x_1 of L_2 at the laser mode λ_2 is then made to interfere with a constant bias signal, resulting in the term $x_2 = t_a x_1 + t_b$. Next, the signal propagates through the optical isolator into the GCSOA L_1 as the feedback signal of the amplifier at λ_2 and interacts with the laser mode λ_1 ($x_3 = \sqrt{E_{0L1}^2 - |x_2|^2}$). Finally x_3 interferes with the bias signal t_b closing the feedback loop and resulting in $x = t_a x_3 + t_b$. Substituting the intermediate signals recursively gives the feedback equation of the structure for the electric field x in Fig. 4.3 going into GCSOA L_2 at frequency λ_1:

$$x = t_a \sqrt{E_{0L1}^2 - \left| t_a \sqrt{E_{0L2}^2 - |x|^2} + t_b \right|^2} + t_b. \tag{4.9}$$

The left and right hand sides of (4.9) give the input x before and after a round trip through the device. If both sides of (4.9) are equal (ie the input x is the same before and after a round trip), the state of the system remains unchanged. If the delayed input (right hand side) is larger than the stimulus x, it then follows that x grows with time until (4.9) is satisfied. Similarly, if the delayed input is smaller than the input x, then x must decrease with time until (4.9) is fulfilled. From these facts it follows that the system is stable when (4.9) is satisfied, and the derivative of the right hand side is < 1. If (4.9) is satisfied but the derivative is > 1 the system is in a labile state and starts to converge towards a stable state. Figure 4.4 illustrates the stable and labile areas of operation.

Injecting an additional input signal to L_1 or L_2 reduces the maximum fields E_{0L1} and E_{0L2} of the GCSOAs, respectively. When the input signal is strong enough and one of the parameters, E_{0L1} or E_{0L2}, is reduced below a threshold value, one of the stable states disappears and the system is left with only one stable state. Graphical solution of Eq. (4.9) and the transition from a bistable system to a monostable system is illustrated in Fig. 4.4. The existence of the monostable regime allows setting or resetting the COFF by simply injecting an optical signal into GCSOA L_1 or L_2.

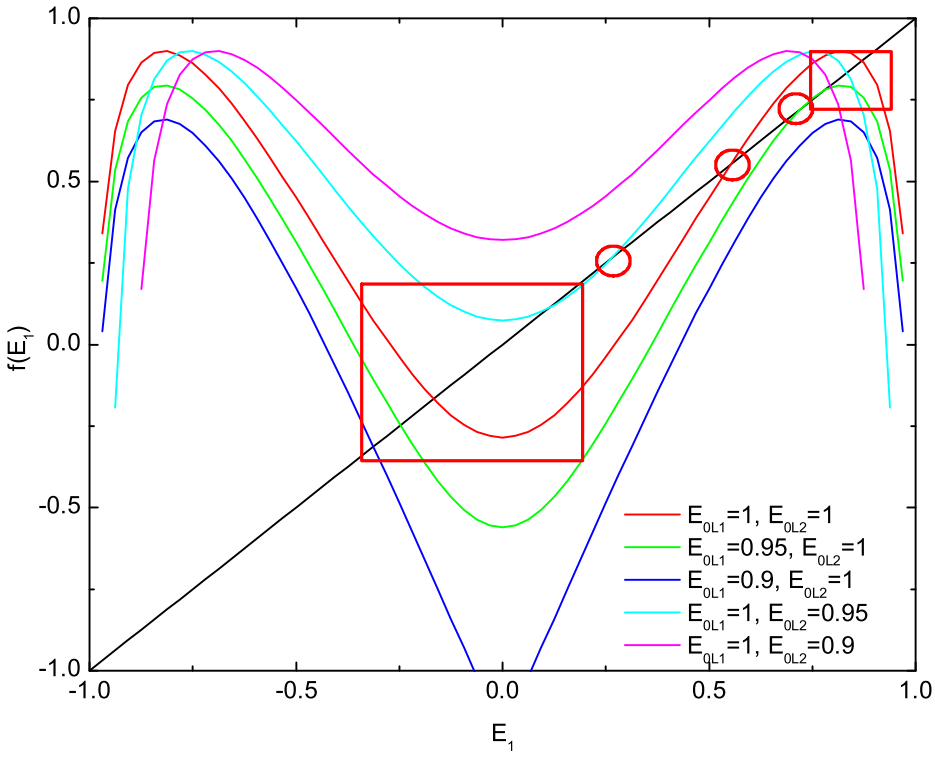

Figure 4.4: Graphical solutions of the feedback equation (4.9) of the flip-flop for different values of E_{L01} and E_{L02}. The black curve is the left hand side of Eq. (4.9). The red curve is drawn for the case of no input power in the set or reset port ($E_{L01} = E_{L02} = 1$). Other values of E_{L01} and E_{L02} describe the cases where an input signal is present in the set or reset port of the flip-flop. The stable (labile) operating points of the flip-flop are located inside the rectangles (circles) at the crossings of the curves with the black curve. For the two extreme curves ($E_{0L1} = 1$, $E_{0L2} = 0.9$ and $E_{0L1} = 0.9$, $E_{0L2} = 1$) there is only one stable state left, and the flip-flop will move to this state.

4.2.1 The rate equation model of the optical flip-flops

The dynamics of the COFF can be modeled by a set of coupled rate equations that describe the carrier densities and electric field phasors of the pertinent GCSOAs. The equations resemble closely the rate equations (3.5) and (3.7) of a single phase locked laser, but the carrier density $\mathbf{n}_e$ and the electric fields $\mathbf{E}_j$ and $\mathbf{E}_j^{\text{ext}}$ are now vectors whose components describe the quantity in question in each GCSOA of the system. The equations are not crucial for understanding the principle of operation of the COFF, and they are only discussed very briefly and partly incompletely in this summary. For further details the reader

is referred to publications III-VI.

The rate equations for a general coherent nonlinear system can be written in vector form as

$$\frac{d\mathbf{n}_e}{dt} = \frac{I}{qV} - \sum_{j\in\{1,2,3\}} 2\xi c\mathbf{g}_j\left(\mathbf{n}_e\right)\left|\mathbf{E}_j\right|^2 - \frac{\mathbf{n}_e}{\tau} \tag{4.10}$$

$$\begin{aligned}\frac{d\mathbf{E}_j}{dt} &= \frac{c}{2}\left[\mathbf{g}_j\left(\mathbf{n}_e\right) - \boldsymbol{\alpha}_j + i\Delta\boldsymbol{\omega}_j\left(\mathbf{n}_e\right)\right]\mathbf{E}_j \\ &\quad + \frac{c}{2L}\mathbf{E}_j^{\text{ext}} + \frac{c}{2L}\mathbf{M}_j\mathbf{E}_j\end{aligned} \tag{4.11}$$

where the gain $\mathbf{g}_j$, absorption $\boldsymbol{\alpha}_j$ and frequency detuning $\Delta\boldsymbol{\omega}_j$ are correspondingly diagonal matrices. The diagonal elements give the values of the respective quantities for each GCSOA. Index j denotes the mode of the GCSOA (here $j \in \{1,2,3\}$). The coupling matrices $\mathbf{M}_j$ describe the coupling of the laser fields between the different GCSOAs. The term $\xi = \sqrt{\varepsilon\mu^{-1}}/\left(2\hbar\omega c\right)$ is the conversion factor that transforms the square of the absolute value of the electric field to photon density. The factor 2 in front of ξ in Eq. (4.10) results from the presence of the two counter propagating electric fields both contributing to the photon density. The absolute value in Eq. (4.10) is applied to each component of $\mathbf{E}_j$ independently. The vector $\mathbf{E}_j^{\text{ext}}$ describes the fields injected from outside the cavity into the mode j. Other parameters have the same significance as in Eqs. (3.5) and (3.7).

To model the COFF composed of two GCSOAs, presented in Subsection 4.2, the following parameter values are used:

$$\mathbf{M}_1 = \sqrt{T_L T_s}\begin{bmatrix} 0 & t_a \\ 0 & 0 \end{bmatrix} \tag{4.12}$$

$$\mathbf{M}_2 = \sqrt{T_L T_s}\begin{bmatrix} 0 & 0 \\ t_a & 0 \end{bmatrix} \tag{4.13}$$

$$\mathbf{M}_3 = \mathbf{0} \tag{4.14}$$

$$\mathbf{E}_1^{\text{ext}} = \sqrt{T_s}\begin{bmatrix} t_b & 0 \end{bmatrix}^{\text{T}} E_{L,\max}^{\text{out}} \tag{4.15}$$

$$\mathbf{E}_2^{\text{ext}} = \sqrt{T_s}\begin{bmatrix} 0 & t_b \end{bmatrix}^{\text{T}} E_{L,\max}^{\text{out}} \tag{4.16}$$

$$\mathbf{E}_3^{\text{ext}} = \sqrt{T_s}\begin{bmatrix} s_S\left(t\right) & s_R\left(t\right) \end{bmatrix}^{\text{T}} \tag{4.17}$$

$$\boldsymbol{\alpha}_1 = \begin{bmatrix} \alpha_L & 0 \\ 0 & \alpha_s \end{bmatrix} \tag{4.18}$$

$$\boldsymbol{\alpha}_2 = \begin{bmatrix} \alpha_s & 0 \\ 0 & \alpha_L \end{bmatrix} \tag{4.19}$$

$$\boldsymbol{\alpha}_3 = \begin{bmatrix} \alpha_s & 0 \\ 0 & \alpha_s \end{bmatrix}. \tag{4.20}$$

The parameters T_L, T_s and α_L and α_s ($\alpha_s > \alpha_L$) describe the effective transmittance of the cavity facets and the cavity losses of the laser mode and of the signal mode, respectively. The set and reset signals $s_S(t)$ and $s_R(t)$ are used to switch the state. The parameters t_a and t_b are configured so that the device operates with the desired properties and are normalized so that the maximum output electric field $E^{\text{out}}_{L,\text{max}}$of the laser mode can be used as a reference value. Numerical values for the parameters can be found in Publication V.

The results obtained for parametrized structures, that are optimistic but within the limits of current technological feasibility, show that the COFFs can be operated at frequencies well above 40 GHz. Theoretically the operating frequency can be increased along with the optical power and differential gain of the GCSOA, towards the fundamental upper limit $\sim v(\alpha_s - G_s)/20$ (or $\sim v\alpha_L$ if it is smaller) which depends on the cavity losses and available material gain.

Two examples of typical results obtained by using the rate equation model are shown in Figs. 4.5 and 4.6. In Fig. 4.5 the output of the COFF is shown as a function of the input power in the set -port. There is a very clear threshold for the input power for the COFF to change state. In Fig. 4.6 the dynamic operation of the COFF is demonstrated for set and reset -pulses. After setting (resetting) the COFF, its state remains unchanged until a reset (set) pulse is sent to the input.

4.3 Active antireflectors

Because optical isolators that are suitable for integration are presently not available, other means to prevent unwanted signals from reaching the GCSOAs of the COFF are needed.

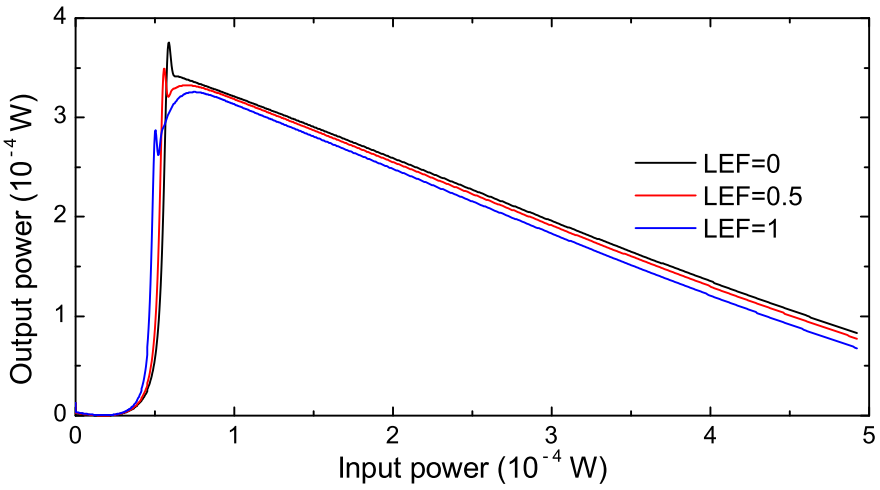

Figure 4.5: When a sufficient input power is injected in the set-port, the output power in the output port of the COFF rises abruptly, as predicted by the feedback equation (4.9). The threshold for changing the state is very clear. With increasing input power, however, the output power decreases slowly, which may be a minor drawback in some applications. The results shown here are calculated using the more accurate rate equation model for a slowly changing input signal (see Publications IV and V for details).

The components preventing backward propagation of signals in this thesis, however, need not necessarily be optical isolators – antireflectors satisfy the requirements as well.

The reflection of any optical signal $S(t)$ that is transformed and reflected back as $f(S)$ by some optical device, linear or nonlinear, can be cancelled by destructive interference using another replica of the response $f(S)$ (Fig. 4.7). Creating the replica can be done by approximating the response f, or, for better cancellation, by using a duplicate of the device creating the reflection. The performance of the antireflector is limited by the accuracy of the phase shift and the (anti)symmetry of the antireflector structure.

Using the principle of antireflection allows one to modify the COFF structure into a form that is in principle suitable for integration, as described in Fig. 4.8. This configuration has been used in all the calculations in publications IV-VI. The drawback of using antireflectors is that they add to the complexity of the COFF configuration.

Accounting for the antireflectors and the lasers providing the bias signals and phase

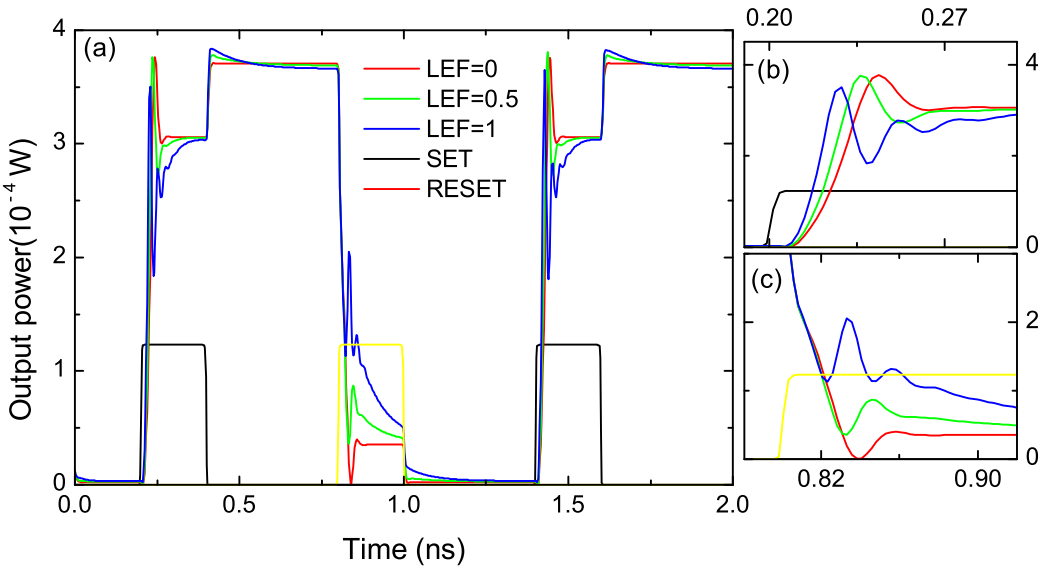

Figure 4.6: Sending input signals into the COFF nicely demonstrates the operation as a memory unit. The output power rises abruptly when a set-pulse is sent into the set-port. Even when the set-pulse disappears, the output power remains close to the value set by the pulse. Resetting the COFF can only be done by using a reset-pulse. The insets show a magnification of the output at the moment of (b) setting and (c) resetting the COFF.

locking signals in the rate equation model presented in Section 4.2.1 results in the coupling matrices of the form

$$\mathbf{M}_1 = \begin{bmatrix} 0 & C & iC & iB & B & 0 \\ C & 0 & 0 & iA & A & 0 \\ iC & 0 & 0 & 0 & 0 & 0 \\ iB & iA & 0 & 0 & 0 & 0 \\ B & A & 0 & 0 & 0 & 0 \\ 0 & 0 & 0 & 0 & 0 & 0 \end{bmatrix} \tag{4.21}$$

$$(\mathbf{M}_2)_{n,m} = (\mathbf{M}_1)_{7-n,7-m} \tag{4.22}$$

$$\mathbf{M}_3 = \mathbf{0} \tag{4.23}$$

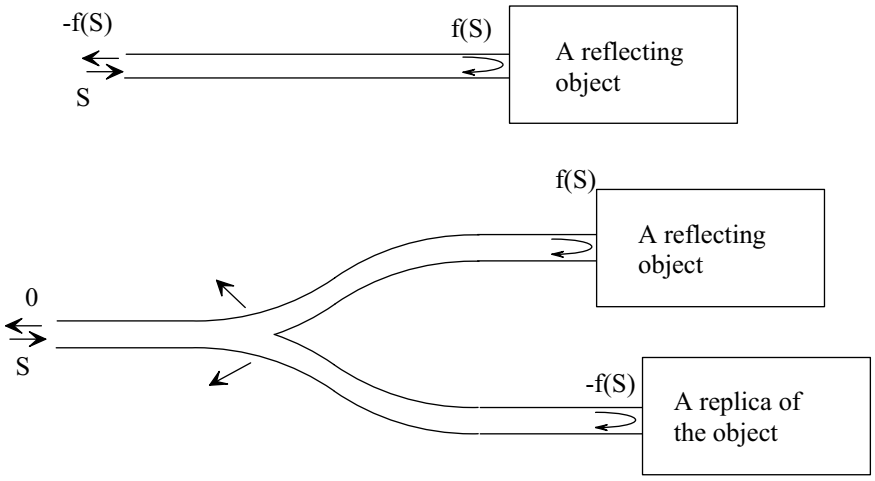

Figure 4.7: Availability of optical isolators in integrated environments is severely limited. Active antireflectors can be used to replace optical isolators in systems where a replica of the reflected signal can be created. The reflection from an object that reflects a forward propagating signal S back as $f(S)$ may be cancelled by interference if a replica of the reflected signal can be created and made to interfere with the original reflection destructively.

$$A = \frac{1}{4}\sqrt{T_L T_s}\, g_A t_A^2 \tag{4.24}$$

$$B = \frac{1}{4\sqrt{2}}\sqrt{T_L T_s}\, g_A t_A t_B \tag{4.25}$$

$$C = \frac{1}{2} T_L t_C. \tag{4.26}$$

The elements of the matrices and vectors are associated to the lasers L_{B1}, L_1, L_{A1}, L_{A2}, L_2 and L_{B2} of Fig. 4.8, respectively. Again, the effective transmission coefficients of the cavity facets for the laser and signal modes are given by T_L and T_s, respectively. The terms t_A, t_B and t_C are the waveguide transmission coefficients for the electric field (Fig. 4.8) and g_A is the amplification of the electric field in the optional amplifier compensating for the losses of the waveguide junctions. The vectors describing the external injection (set and reset signals) are zero, except for

$$\mathbf{E}_3^{\text{ext}} = \left[\begin{array}{cccccc} 0 & s_S(t) & i\, s_S(t) & i\, s_R(t) & s_R(t) & 0 \end{array}\right]^{\mathrm{T}}.$$

The loss matrix $\boldsymbol{\alpha}_j$ of each GCSOA is diagonal and given by

$$\boldsymbol{\alpha}_1 = \mathrm{Diag}\left[\begin{array}{cccccc} \alpha_L & \alpha_L & \alpha_L & \alpha_s & \alpha_s & \alpha_s \end{array}\right]$$

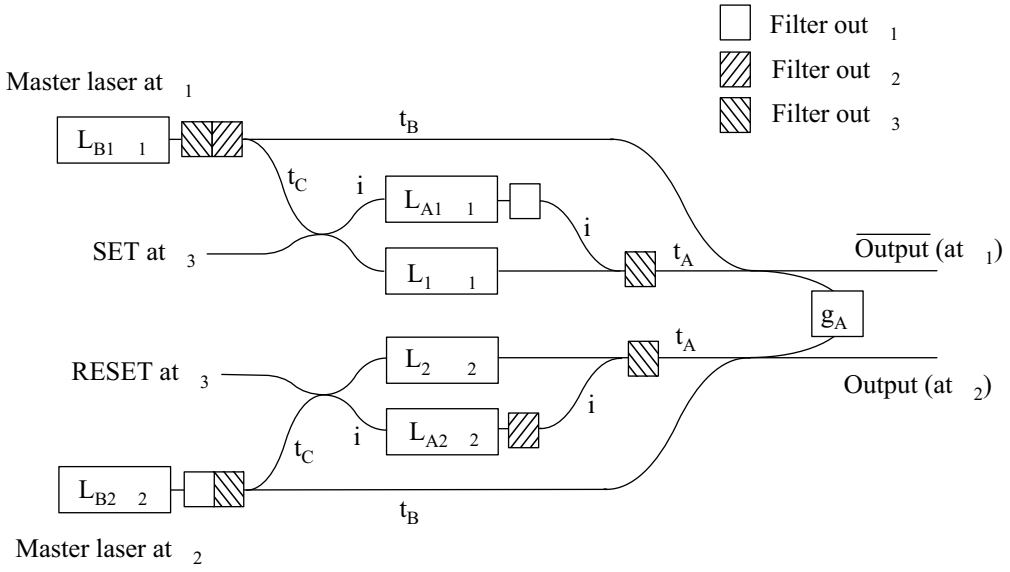

Figure 4.8: The full COFF configuration with antireflectors no longer uses optical isolators. They have been replaced by active antireflectors that are able to cancel the reflections from the GCSOAs L_1 and L_2. The structure also includes two lasers that provide bias signals and phase locking for the system. The state of the COFF can be changed by applying a signal to the set or reset input port, and the output or the inverted output can be read from the respective output ports.

$$\boldsymbol{\alpha}_2 = \mathrm{Diag}\left[\begin{array}{cccccc} \alpha_s & \alpha_s & \alpha_s & \alpha_L & \alpha_L & \alpha_L \end{array}\right]$$

$$\boldsymbol{\alpha}_3 = \mathrm{Diag}\left[\begin{array}{cccccc} \alpha_s & \alpha_s & \alpha_s & \alpha_s & \alpha_s & \alpha_s \end{array}\right]$$

where the operator Diag constructs a diagonal matrix from the vector following it. Numerical values can be found in publication V.

4.4 Optical decision circuits and logic

The basic COFF has two stable states when no external input signals are present. In presence of an appropriate set or reset signal only one stable state remains, enabling the set and reset operations of the memory. Making the COFF structure asymmetric by adjusting the injection current or the strength of the feedback from GCSOA L_1 to L_2 to be different from the feedback from L_2 to L_1 leads to a similar situation. With a suitable amount of asymmetry only one stable state remains even when an input signal is not present. An

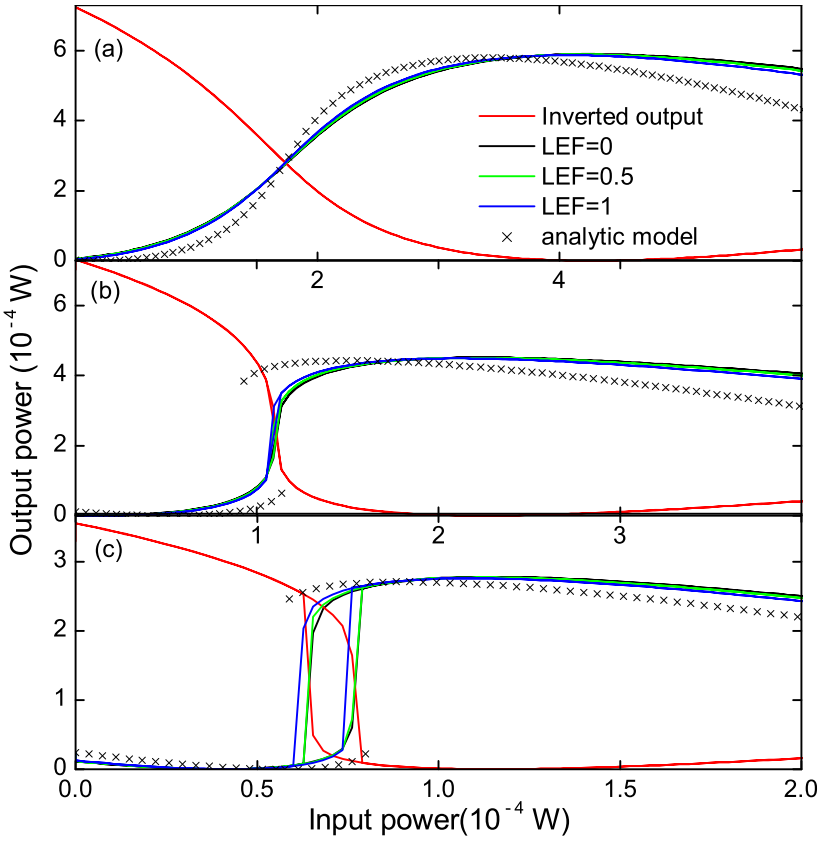

Figure 4.9: Steady state characteristics of three different decision circuit configurations. The curves are calculated both analytically using Eq. (4.27) and numerically using the rate equation model introduced in Publication V for various values of LEF. The steepness and hysteresis of the decision threshold can be affected by the device parameters, which describe the feedback strength between the amplifiers. In (a) the parameters are such that the threshold is gentle, while in (b) and (c) the threshold is steep. In (b) hysteresis is visible in the analytical approximation but not in the more accurate numerical simulation. In (c) hysteresis is present in both the analytical and numerical results.

input signal to the GCSOA L_1 (or L_2 depending on how the feedback was modified) can then be injected to reduce the output power of the laser mode. As a result the stability conditions change so that first, at moderate input power, a second stable state is created. Then, when the input power reaches a threshold, the original stable state disappears and the system is driven to the newly created stable state which is different from the original stable state. The disappearance of the stable state takes place abruptly, which makes the

asymmetrically adjusted COFF suitable for use as a decision circuit.

Introducing the asymmetry to the feedback equation (4.9) in the form of modified feedback and bias signal strengths t_{a1}, t_{a2}, t_{b1} and t_{b2} transforms the feedback equation into

$$x = t_{a1}\sqrt{E_{0L1}^2 - \left|t_{a2}\sqrt{E_{0L2}^2 - |x|^2} + t_{b2}\right|^2} + t_{b1} \tag{4.27}$$

which is different from the original feedback equation (4.9) of the COFF only by the asymmetric feedback parameters and the different maximum laser fields of the GCSOA. However, the system may now be monostable and returns quickly to its unexcited stable state when an input signal drops below a threshold value, as shown in Fig. 4.9. The dynamical properties of the decision circuit remain similar to those of the basic COFF circuit.

A decision circuit with steep threshold characteristics is not only useful in regeneration of optical signals, but also in constructing logic gates. Creating an and gate or an or gate only requires a two arm interferometer in addition to a decision circuit with a steep decision threshold. The output power of an interferometer followed by a threshold circuit is given by

$$P_{\text{out}} = f\left[\xi\left|E_A + E_B\right|^2\right] \tag{4.28}$$

where $f\left(P\right)$ is the response of the decision circuit. The output has different properties depending on the phase difference θ of the input signals. If the signals E_A and E_B are in phase, and-like output is obtained. With phase difference of about 110° the response resembles the logical or function. Fig. 4.10 shows some examples of the responses of the logic circuits realized with the decision circuits of Figs. 4.9(b) and 4.9(c).

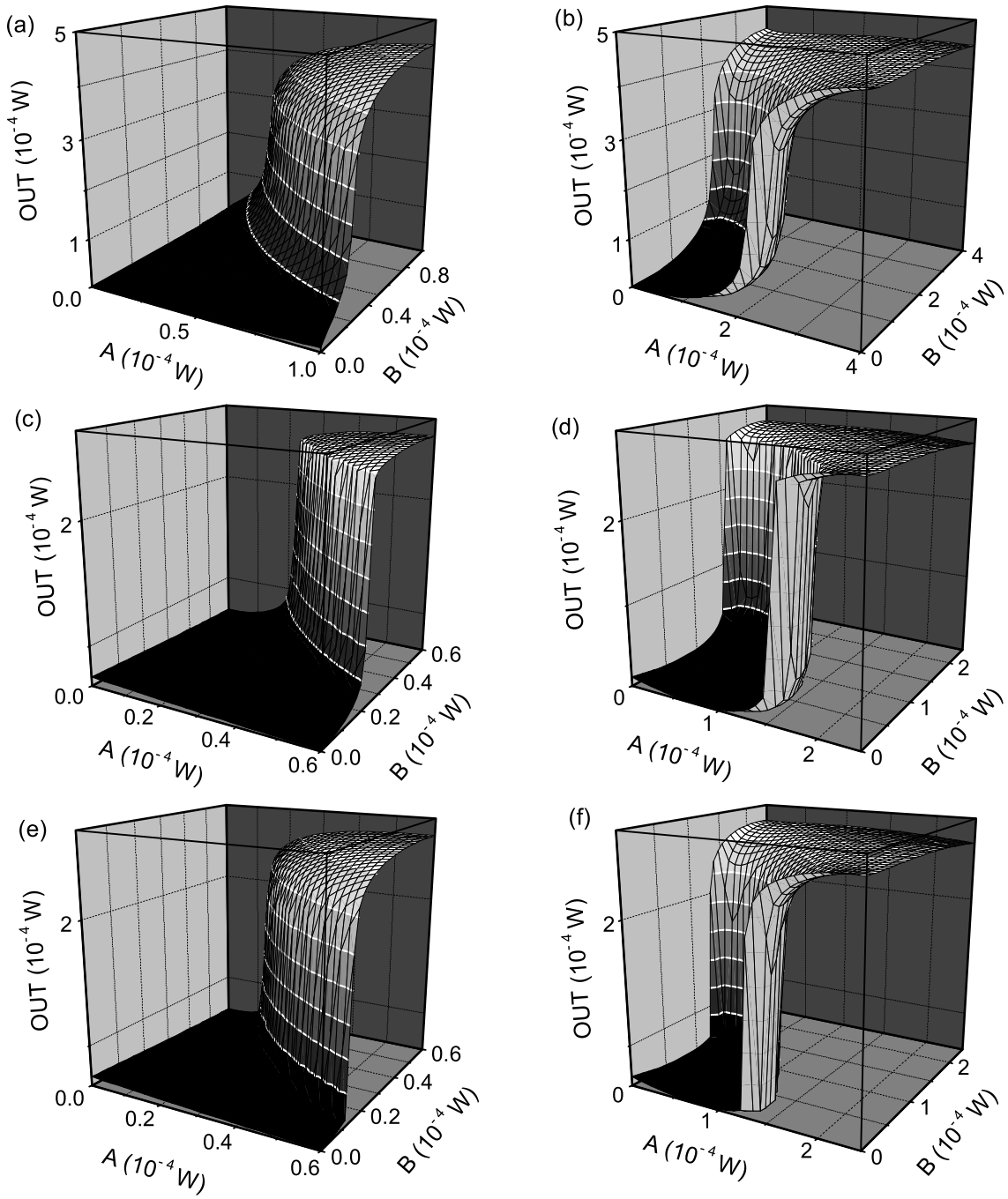

Figure 4.10: The two dimensional truth tables of the and (left) and or (right) gates for input signals A and B realized with an interferometer and the threshold circuits of Figs. 4.9(b) [(a) and (b)] and 4.9(c) [(c) and (d) for the lower hysteresis curve of Fig. 4.9(c) and (e) and (f) for the upper hysteresis curve]. For and gates constructive interference in the interferometer is used ($\theta = 0$) and for the or gates $\theta = 110°$. Although the output is circularly symmetric, it provides a fairly good approximation of the ideal truth table.

5 Conclusions

In the future optical networks will continue expanding and getting closer to the end user as the bandwidth requirements increase. The new optical components developed in the laboratories will be adopted and commercialized by the telecommunications industry only when they are cost effective. Other fields of technology, where very fast serialized data transfer is needed and cost-effectiveness does not play so crucial a role is a potential stepping stone for the more complex new optical components on their way to mass production. The new components might find their first applications for example in the communication links between the nodes of a supercomputer. Thereafter, as the technology matures and costs decrease, they may become commercially available for optical networks as well.

The progress made in the laser materials, modulators, amplifiers and optical fibers are all important steps on the way to better devices and systems. The introduction of quantum wells and dots as the active material in lasers has improved several operation characteristics of semiconductor lasers. Integrated optical amplifiers with gain clamping have linearized the amplification. The losses in optical fibers have become almost negligible and the dispersion in the fibers can be controlled.

The most salient problem of today's optical networks, and transferring data optically in general, is the so called electronic bottleneck. It emerges from the need to convert optical signals into electric form and back for routing, retiming or processing. In laboratories all over the world many different methods and components to help overcoming the electronic bottleneck have been proposed. However, no fast commercial breakthrough is at sight for the moment.

Coherent optics is sometimes dismissed as a research topic by the networking industry. In networks involving optical fibers this is easily justified, since it is impossible to accurately control all conditions affecting the optical properties and optical phase of the system. In integrated circuits, however, the situation is somewhat different. In small scale local coherence is and has long been an essential part of many modulators and nonlinear devices, since they depend on interference of optical signals. In this thesis the use of local coherence is extended to a small group of phase locked lasers connected by

waveguides. The key result is a new form of nonlinearity obtained by interferometry and GCSOAs. The nonlinearity is used to theoretically demonstrate an optical flip-flop that uses coherent signals internally, but communicates with the external world using intensity only.

This thesis has been devoted to the study of the dynamical properties of quantum dot lasers and gain clamped optical amplifiers and their use with interferometers to create a new type of nonlinearity for nonlinear optical circuits. The study of quantum dot lasers was done with particular interest in the linewidth enhancement factor. In the literature it is commonly stated that ideally the LEF of QDLs is inherently small because of the symmetry of the inhomogeneously broadened density of states. This turned out to be an inaccurate approximation even in ideal conditions. The signal propagation in LOAs was also studied and compared to the conventional GCSOAs and SOAs. The superiority of the linearity and crosstalk properties in the LOAs with respect to the properties of SOAs was verified. Most of the attention in the summary and the publications, however, is given to the introduction of an optical flip-flop circuit and related devices that have been realized using nonlinear feedback formed by GCSOAs and interferometers.

In the very best possible scenario, coherent optical devices developed from the devices introduced in this thesis may become as versatile tools for optics as the transistors are for electronics. Coherent optics have the potential for high speed operation, now obtaining possibly ~ 100 GHz operating frequency with the current level of technology and perhaps even THz or tens of THz in the future. Processing the devices is challenging, but in principle possible even with today's technology. The differences between the flip-flops and logic circuits are so small that only a few extra steps are needed to process both on the same chip. The power consumption is at least slightly elevated and the footprint is huge in comparison to electronic transistors. The footprint is ultimately limited by the wavelength of optical signals even if using photonic crystal waveguides allowing sharp bends.

The use of GCSOAs is not an optimal choice for the electric field nonlinearity due to its complexity and slow operation in comparison to the interferometers. Being able to replace it with some other means to produce a similar output with a simpler arrangement

would offer a great leap for coherent technology.

All the optical components investigated in this thesis have been separately realized in practice. Combining them on a chip and making them interact coherently is more challenging. Even in theory, there remains several issues, mostly of technological nature, that have not been thoroughly investigated. However, these issues should not be insuperable. Building a prototype on an optical table may be hampered by the need for phase control and by the cavity mode requirements of the GCSOA. Integration of a prototype directly on a chip is even more demanding.

If the manufacturing technology of optical components develops with a pace comparable to that of silicon technology, optical signal processing will meet many of the expectations placed for it in the near future. The co-operation of the optical and electrical technologies will still remain strong for at least a while, but with a few important innovations the purely optical signal processing capabilities may become sufficient by themselves.

References

[1] T. H. Maiman, "Stimulated optical radiation in ruby," *Nature*, vol. 187, pp. 493–494, Aug. 1960.

[2] A. L. Schawlow and C. H. Townes, "Infrared and optical masers," *Phys. Rev.*, vol. 112, no. 6, pp. 1940–1949, Dec. 1958.

[3] A. Javan, J. W. R. Bennett, and D. R. Herriott, "Population inversion and continuous optical maser oscillation in a gas discharge containing a He-Ne mixture," *Phys. Rev. Lett.*, vol. 6, no. 3, pp. 106–110, Feb. 1961.

[4] R. N. Hall, G. E. Fenner, J. D. Kingsley, T. J. Soltys, and R. O. Carlson, "Coherent light emission from GaAs junctions," *Phys. Rev. Lett.*, vol. 9, no. 1, pp. 366–368, Nov. 1962.

[5] M. I. Nathan, W. P. Dumke, G. Burns, J. Frederick H. Dill, and G. Lasher, "Stimulated emission of radiation from GaAs p-n junctions," *Appl. Phys. Lett.*, vol. 1, no. 3, pp. 62–64, Nov. 1962.

[6] P. A. Franken, A. E. Hill, C. W. Peters, and G. Weinreich, "Generation of optical harmonics," *Phys. Rev. Lett.*, vol. 7, no. 4, pp. 118–119, Aug. 1961.

[7] G. Eckhardt, R. W. Hellwarth, F. J. McClung, S. E. Schwarz, D. Weiner, and E. J. Woodbury, "Stimulated Raman scattering from organic liquids," *Phys. Rev. Lett.*, vol. 9, no. 11, pp. 455–457, Dec 1962.

[8] E. J. Woodbury, "Ruby laser operation in near IR," *Proc. IRE*, vol. 50, p. 2367, 1962.

[9] R. Y. Chiao, C. H. Townes, and B. P. Stoicheff, "Stimulated Brillouin scattering and coherent generation of intense hypersonic waves," *Phys. Rev. Lett.*, vol. 12, no. 21, pp. 592–595, May 1964.

[10] G. P. Agrawal, *Nonlinear fiber optics*. Academic Press, San Diego, CA, 1995.

[11] ——, *Fiber-optic communication systems, Second edition*. John Wiley & Sons, Inc, 1997.

[12] H. J. Caulfield, "Perspectives in optical computing," *IEEE Computer*, vol. 31, no. 2, pp. 22–25, Feb. 1998.

[13] A. Jajszczyk, "Optical networks - the electro-optic reality," *Optical switching and networking*, vol. 1, no. 1, pp. 3–18, Jan. 2005.

[14] W. K. H. Panofsky and M. Phillips, *Classical electricity and magnetism*. Addison-Wesley publishing company, 1972.

[15] L. E. Ballentine, *Quantum mechanics: A modern development*. World Scientific Publishing Co. Pte. Ltd, 1998.

[16] R. Loudon, *The quantum theory of light, 2nd edition*. Oxford University Press, 1983.

[17] J. Singh, *Semiconductor optoelectronics, physics and technology*. McGraw-Hill, Inc., 1995.

[18] A. Yariv, *Optical electronics in modern communications, 5th Ed.* Oxford University Press, NY, 1997.

[19] P. Bhattacharya, *Semiconductor optoelectronic devices, Second edition*. Prentice Hall, 1997.

[20] C. H. Henry, "Theory of the linewidth of semiconductor lasers," *IEEE J. Quantum Electron.*, vol. 18, no. 2, pp. 259–264, Feb. 1982.

[21] J.-S. Peng and G.-X. Li, *Introduction to modern quantum optics*. World Scientific Publishing Co. Pte. Ltd., 1998.

[22] R. W. Robinett, *Quantum mechanics: Classical results, modern systems, and visualized examples*. Oxford University Press, 1996.

[23] U. Leonhardt, *Measuring the quantum state of light*. Cambridge University Press, 1997.

[24] J. Singh, *Physics of semiconductors and their heterostructures*. McGraw-Hill, 1993.

[25] R. Ramaswami and K. N. Sivarajan, *Optical networks, A practical perspective*. Morgan Kaufmann Publishers, Inc, 1998.

[26] H. A. Haus, "The noise figure of optical amplifiers," *IEEE Photon. Technol. Lett.*, vol. 10, no. 11, pp. 1602–1604, Nov. 1998.

[27] P. L. Kelley and W. H. Kleiner, "Theory of electromagnetic field measurement and photoelectron counting," *Phys. Rev.*, vol. 136, no. 2A, pp. A316–A334, Oct. 1964.

[28] B. R. Mollow, "Quantum theory of field attenuation," *Phys. Rev.*, vol. 168, no. 5, pp. 1896–1919, Apr 1968.

[29] M. O. Scully and W. E. Lamb, "Quantum theory of an optical maser. III. Theory of photoelectron counting statistics," *Phys. Rev.*, vol. 179, no. 2, pp. 368–374, Mar 1969.

[30] M. Rousseau, "A new quantum mechanical derivation of the photocounting distribution," *J. Phys. A*, vol. A10, no. 6, pp. 1043–1047, 1977.

[31] T. J. Shepherd, "A model for photodetection of single-mode cavity radiation," *J. Mod. Opt*, vol. 28, no. 4, pp. 567 – 583, Apr. 1981.

[32] Y. Suematsu and A. R. Adams, Eds., *Handbook of semiconductor lasers and photonic integrated circuits*. London: Chapman & Hall, 1994.

[33] T. C. Newell, D. J. Bossert, A. Stintz, B. Fuchs, K. J. Malloy, and L. F. Lester, "Gain and linewidth enhancement factor in InAs quantum-dot laser diodes," *IEEE Photon. Technol. Lett.*, vol. 11, no. 12, pp. 1527–1529, Dec. 1999.

[34] A. A. Ukhanov, A. Stintz, P. G. Eliseev, and K. J. Malloy, "Comparison of the carrier induced refractive index, gain and linewidth enhancement factor in quantum dot and quantum well lasers," *Appl. Phys. Lett.*, vol. 84, no. 7, pp. 1058–1060, Feb. 2004.

[35] D. Bimberg, N. Kirstaedter, N. N. Ledentsov, Z. I. Alferov, P. S. Kop'ev, and V. M. Ustinov, "InGaAs-GaAs quantum-dot lasers," *IEEE J. Select. Topics Quantum Electron.*, vol. 3, no. 2, pp. 196–205, Apr. 1997.

[36] C. H. Henry, R. A. Logan, and K. A. Bertness, "Spectral dependence of the change in refractive index due to carrier injection in GaAs lasers," *J. Appl. Phys.*, vol. 52, no. 7, pp. 4457–4461, July 1981.

[37] M. Osiński and J. Buus, "Linewidth broadening factor in semiconductor lasers - an overview," *IEEE J. Quantum Electron.*, vol. 23, no. 1, pp. 9–29, Jan. 1987.

[38] K. Czotscher, S. Weisser, A. Leven, and J. Rosenzweig, "Intensity modulation and chirp of 1.55-μm multiple-quantum-well laser diodes: modeling and experimental verification," *IEEE J. Select. Topics Quantum Electron.*, vol. 5, no. 3, pp. 606–612, May 1999.

[39] S. Ghosh, S. Pradhan, and P. Bhattacharya, "Dynamic characteristics of high-speed $In_{0.4}Ga_{0.6}As$/GaAs," *Appl. Phys. Lett.*, vol. 81, no. 16, pp. 3055–3057, Oct. 2002.

[40] H. Saito, K. Nishi, A. Kamei, and S. Sugou, "Low chirp observed in directly modulated quantum dot lasers," *IEEE Photon. Technol. Lett.*, vol. 12, no. 10, pp. 1298–1300, Oct. 2000.

[41] D. Bimberg, M. Grundmann, and N. N. Ledentsov, *Quantum dot heterostructures*. West Sussex, England: Wiley, 1999.

[42] M. Sugawara, K. Mukai, Y. Nakata, H. Ishikawa, and A. Sakamoto, "Effect of homogeneous broadening of optical gain on lasing spectra in self-assembled $In_xGa_{1-x}As$/GaAs quantum dot lasers," *Phys. Rev. B*, vol. 61, no. 11, pp. 7595–7603, Mar 2000.

[43] M. Grundmann and D. Bimberg, "Gain and threshold of quantum dot lasers: Theory and comparison to experiments," *Jpn. J. Appl. Phys.*, vol. 36, pp. 4181–4187, 1997.

[44] G. Park, O. B. Shchekin, D. L. Huffaker, and D. G. Deppe, "Low-threshold oxide-confined 1.3-μm quantum-dot laser," *IEEE Photon. Technol. Lett.*, vol. 13, no. 3, pp. 230–232, Mar. 2000.

[45] L. F. Lester, A. Stintz, H. Li, T. C. Newell, E. A. Pease, B. A. Fuchs, and K. J. Malloy, "Optical characteristics of 1.24-μm InAs quantum-dot laser diodes," *IEEE Photon. Technol. Lett.*, vol. 11, no. 8, pp. 931–933, Aug. 1999.

[46] M. Asada, Y. Miyamoto, and Y. Suematsu, "Gain and the threshold of three-dimensional quantum-box lasers," *IEEE J. Quantum Electron.*, vol. 22, no. 9, pp. 1915–1921, Sept. 1986.

[47] N. Kirstaedter, O. G. Schmidt, N. N. Ledentsov, D. Bimberg, V. M. Ustinov, A. Y. Egorov, A. E. Zhukov, M. V. Maximov, and P. S. Kop'ev, "Gain and differential gain of single layer InAs/GaAs quantum dot injection lasers," *Appl. Phys. Lett.*, vol. 69, no. 9, pp. 1226–1228, Aug. 1996.

[48] R. Heitz, M. Grundmann, N. N. Ledentsov, L. Eckey, M.Veit, D. Bimberg, V. M. Ustinov, A. Y. Egorov, A. E. Zhukov, P. S. Kop'eV, and Z. I. Alferov, "Multiphonon-relaxation processes in self-organized InAs/GaAs quantum dots," *Appl. Phys. Lett.*, vol. 68, no. 3, pp. 361–363, Jan. 1995.

[49] S. Grosse, J. H. H. Sandmann, G. von Plessen, J. Feldmann, H. Lipsanen, M. Sopanen, J. Tulkki, and J. Ahopelto, "Carrier relaxation dynamics in quantum dots: Scattering mechanisms and state-filling effects," *Phys. Rev. B*, vol. 55, no. 7, pp. 4473–4476, Feb. 1997.

[50] K. Kim, J. Urayama, and T. B. Norris, "Gain dynamics and ultrafast spectral hole burning in In(Ga)As self-organized quantum dots," *Appl. Phys. Lett.*, vol. 81, no. 4, pp. 670–672, July 2002.

[51] S. Malik, E. C. L. Ru, D. Childs, and R. Murray, "Time-resolved studies of annealed InAs/GaAs self-assembled quantum dots," *Phys. Rev. B*, vol. 63, pp. 155 313–1–155 313–6, Mar. 2001.

[52] T. Yamanaka, Y. Yoshikuni, K. Yokoyama, W. Lui, and S. Seki, "Theoretical study on enhanced differential gain and extremely reduced linewidth enhancement factor in quantum well lasers," *IEEE J. Quantum Electron.*, vol. 29, no. 6, pp. 1609–1616, June 1993.

[53] F. Mogensen, H. Olesen, and G. Jacobsen, "Locking conditions and stability properties for semiconductor laser with external light injection," *IEEE J. Quantum Electron.*, vol. 21, no. 7, pp. 784–793, July 1985.

[54] R. Lang, "Injection locking properties of a semiconductor laser," *IEEE J. Quantum Electron.*, vol. 18, no. 6, pp. 976–983, June 1982.

[55] O. Kjebon, R. Shatz, S. Lourdudoss, S. Nilsson, B. Stålnacke, and L. Bäckbom, "30 GHz direct modulation bandwidth in detuned loaded InGaAsP DBR lasers at 1.55 μm wavelength," *Electr. lett.*, vol. 33, no. 6, pp. 488–499, Mar. 1997.

[56] F. Smith and T. King, *Optics and photonics - An introduction*. John Wiley & Sons, 2000.

[57] M. N. Islam, "Raman amplifiers for telecommunications," *IEEE J. Select. Topics Quantum Electron.*, vol. 8, no. 3, pp. 548–559, May 2002.

[58] S. Verspurten, G. Morthier, and R. Baets, "Experimental and numerical small-signal analysis of two types of gain-clamped semiconductor optical amplifiers," *IEEE J. Quantum Electron.*, vol. 42, no. 3, pp. 302–312, Mar. 2006.

[59] C.-Y. Jin, Y.-Z. Huang, L.-J. Yu, and S.-L. Deng, "Numerical and theoretical analysis of the crosstalk in linear optical amplifiers," *IEEE J. Quantum Electron.*, vol. 41, no. 5, pp. 636–641, May 2005.

[60] G. L. Cariolaro, P. Franco, M. Midrio, and G. L. Pierobon, "Complete statistical characterization of signal and noise in optically amplified fiber channels," *IEEE J. Quantum Electron.*, vol. 31, no. 6, pp. 1114–1122, June 1995.

[61] A. Schell and R. Barakat, "Approach to equilibrium of single mode radiation in a cavity," *J. Phys.*, vol. A6, pp. 626–836, 1973.

[62] K. Shimoda, H. Takahasi, and C. H. Townes, "Fluctuations in amplification of quanta with application to maser amplifiers," *J. Phys. Soc. Jap.*, vol. 12, no. 6, pp. 686–700, June 1957.

[63] D. G. Kendall, "On the generalized "birth-and-death" process," *Ann. Math. Stat.*, vol. 19, no. 1, pp. 1–15, Mar. 1948.

[64] P. Diament and M. C. Teich, "Evolution of the statistical properties of photons passed through a traveling-wave laser amplifier," *IEEE J. Quantum Electron.*, vol. 28, no. 5, pp. 1325–1334, May 1992.

[65] T. Li and M. C. Teich, "Photon point process for traveling-wave laser amplifiers," *IEEE J. Quantum Electron.*, vol. 29, no. 9, pp. 2568–2578, Sept. 1993.

[66] S. Donati and G. Giuliani, "Noise in an optical amplifier: Formulation of a new semiclassical model," *IEEE J. Quantum Electron.*, vol. 33, no. 9, pp. 1481–1488, 1997.

[67] G. Giuliani, "Semiclassical particle-like description of optical amplifier noise," *Opt. Quantum Elect.*, vol. 31, pp. 367–376, 1999.

[68] Y. Yamamoto and K. Inoue, "Noise in amplifiers," *J. Lightwave Technol.*, vol. 21, no. 11, pp. 2895–2915, 2003.

[69] E. L. Wooten, K. M. Kissa, A. Yi-Yan, E. J. Murphy, D. A. Lafaw, P. F. Hallemeier, D. Maack, D. V. Attanasio, D. J. Fritz, G. J. McBrien, and D. E. Bossi, "A review of

lithium niobate modulators for fiber-optic communications systems," *IEEE J. Select. Topics Quantum Electron.*, vol. 6, no. 1, pp. 69–82, Jan. 2000.

[70] M. Soljačić and J. D. Joannopoulos, "Enhancement of nonlinear effects using photonic crystals," *Nature Materials*, vol. 3, pp. 211–219, Apr. 2004.

[71] K. Gallo, G. Assanto, K. R. Parameswaran, and M. M. Fejer, "All-optical diode in a periodically poled lithium niobate waveguide," *Appl. Phys. Lett.*, vol. 79, no. 3, pp. 314–316, July 2001.

[72] C. G. Trevino-Palacios, G. I. Stegeman, and P. Baldi, "Spatial nonreciprocity in waveguide second-order processes," *Opt. Lett.*, vol. 21, no. 18, pp. 1442–1444, sep 1996.

[73] J. Fujita, M. Levy, R. M. Osgood, Jr, L. Wilkens, and H. Dötsch, "Waveguide optical isolator based on Mach-Zehnder interferometer," *Appl. Phys. Lett.*, vol. 76, no. 16, pp. 2158–2160, Apr. 2000.

[74] W. V. Parys, B. Moeyersoon, D. V. Thourhout, R. Baets, M. Vanwolleghem, B. Dagens, J. Decobert, O. L. Gouezigou, D. Make, R. Vanheertum, and L. Lagae, "Transverse magnetic mode nonreciprocal propagation in an amplifying AlGaInAs/InP optical waveguide isolator," *Appl. Phys. Lett.*, vol. 88, pp. 071 115–1–071 115–3, 2006.

[75] V. R. Almeida, C. A. Barrios, R. R. Panepucci, and M. Lipson, "All-optical control of light on a silicon chip," *Nature*, vol. 431, pp. 1081–1084, Oct. 2004.

[76] G. I. Papadimitriou, C. Papazoglou, and A. S. Pomportsis, "Optical switching: Switch fabrics, techniques and architectures," *J. Lightwave Technol.*, vol. 21, no. 2, pp. 384–405, Feb. 2003.

[77] K. Vyrsokinos, G. Toptchiyski, and K. Petermann, "Comparison of gain clamped and conventional semiconductor optical amplifiers for fast all-optical switching," *J. Lightwave Technol.*, vol. 20, no. 10, pp. 1839–1846, Oct. 2002.

[78] W. D'Oosterlinck, G. Morthier, M. K. Smit, and R. Baets, "Very steep optical thresholding characteristic using a DFB laser diode and an SOA in an optical feedback scheme," *J. Lightwave Technol.*, vol. 17, no. 3, pp. 642–644, Mar. 2005.

[79] O. Leclerc, B. Lavigne, E. Balmefrezol, P. Brindel, L. Pierre, D. Rouvillain, and F. Sequineau, "Optical regeneration at 40 Gb/s and beyond," *J. Lightwave Technol.*, vol. 21, no. 11, pp. 2779–2790, Nov. 2003.

[80] A. Kuramoto and S. Yamashita, "All-optical regeneration using a side-mode injection-locked semiconductor laser," *IEEE J. Select. Topics Quantum Electron.*, vol. 9, no. 5, pp. 1283–1287, Sept. 2003.

[81] S. Yamashita, "All-optical 2R regeneration using a two-mode injection-locked Fabry-Pérot laser diode," *IEEE Photon. Technol. Lett.*, vol. 16, no. 4, pp. 1176–1178, Apr. 2004.

[82] D. Wolfson, A. Kloch, T. Fjelde, C. Janz, B. Dagens, and M. Renaud, "40-Gb/s all-optical wavelength conversion, regeneration and demultiplexing in an SOA-based all-active Mach-Zehnder interferometer," *IEEE Photon. Technol. Lett.*, vol. 12, no. 3, pp. 332–334, Mar. 2000.

[83] G. Morthier, M. Zhao, B. Vanderhaegen, and R. Baets, "Experimental demonstration of an all-optical 2R regenerator with adjustable decision threshold and 'true' regeneration characteristics," *IEEE Photon. Technol. Lett.*, vol. 12, no. 11, pp. 1516–1518, Nov. 2000.

[84] K. E. Stubkjaer, "Semiconductor optical amplifier-based all-optical gates for high-speed optical processing," *IEEE J. Select. Topics Quantum Electron.*, vol. 6, no. 6, pp. 1428–1435, Nov. 2000.

[85] A. Hamié, A. Sharaiha, M. Guégan, and B. Pucel, "All-optical logic NOR gate using two-cascaded semiconductor optical amplifiers," *IEEE Photon. Technol. Lett.*, vol. 14, no. 10, pp. 1439–1441, Oct. 2002.

[86] J. H. Kim, Y. M. Jhon, Y. T. Byun, S. Lee, D. H. Woo, and S. H. Kim, "All-optical XOR gate using semiconductor optical amplifiers without additional input beam," *IEEE Photon. Technol. Lett.*, vol. 14, no. 10, pp. 1436–1438, Oct. 2002.

[87] T. Yabu, M. Geshiro, T. Kitamura, K. Nishida, and S. Sawa, "All-optical logic gates containing a two-mode nonlinear waveguide," *IEEE J. Quantum Electron.*, vol. 38, no. 1, pp. 37–46, Jan. 2002.

[88] A. Bogoni, L. Potí, R. Proietti, G. Meloni, F. Ponzini, and P. Ghelfi, "Regenerative and reconfigurable all-optical logic gates for ultra-fast applications," *Electr. lett.*, vol. 41, no. 7, pp. 435–436, Mar. 2005.

[89] T. A. Ibrahim, R. Grover, L.-C. Kuo, S. Kanakaraju, L. C. Calhoun, and P.-T. Ho, "All-optical AND/NAND logic gates using semiconductor microresonators," *IEEE Photon. Technol. Lett.*, vol. 15, no. 10, pp. 1422–1424, Oct. 2003.

[90] K. R. Parameswaran, M. Fujimura, M. H. Chou, and M. M. Fejer, "Low-power all-optical gate based on sum frequency mixing in APE waveguides in PPLN," *IEEE Photon. Technol. Lett.*, vol. 12, no. 6, pp. 654–656, June 2000.

[91] N. Calabretta, Y. Liu, F. M. Huijskens, M. T. Hill, H. de Waardt, G. D. Khoe, and H. J. S. Dorren, "Optical signal processing based on self-induced polarization rotation in a semiconductor optical amplifier," *J. Lightwave Technol.*, vol. 22, no. 2, pp. 372–381, Feb. 2004.

[92] H. Soto, C. A. Díaz, J. Topomondzo, D. Erasme, L. Schares, and G. Guekos, "All-optical AND gate implementation using cross-polarization modulation in a semiconductor optical amplifier," *IEEE Photon. Technol. Lett.*, vol. 14, no. 4, pp. 498–500, Apr. 2002.

[93] A. Szöke, J. Daneu, J. Goldhar, and N. A. Kurnit, "Bistable optical element and its applications," *Appl. Phys. Lett.*, vol. 15, no. 11, pp. 376–379, Dec. 1969.

[94] P. Blixt and U. Öhlander, "19 ps switching of a bistable laser diode with 30 fJ optical pulses," *IEEE Photon. Technol. Lett.*, vol. 2, no. 3, pp. 175–177, Mar. 1990.

[95] J.-Y. Wang, M. Cada, R. V. Dommelen, and T. Makino, "Dynamic characteristics of bistable laser diodes," *IEEE J. Select. Topics Quantum Electron.*, vol. 3, no. 5, pp. 1271–1279, Oct. 1997.

[96] F. Robert, D. Fortusini, and C. L. Tang, "All-optical set-reset operation of a bistable semiconductor laser intracavity-coupled to a vertical cavity surface-emitting laser," *IEEE Photon. Technol. Lett.*, vol. 12, no. 5, pp. 465–467, May 2000.

[97] M. T. Hill, H. de Waardt, G. D. Khoe, and H. J. Dorren, "All-optical flip-flop based on coupled laser diodes," *IEEE J. Quantum Electron.*, vol. 37, no. 3, pp. 405–413, Mar. 2001.

[98] M. T. Hill, H. de Waardt, G. D. Khoe, and H. J. S. Dorren, “Fast optical flip-flop by use of Mach-Zehnder interferometers,” *Microwave and Optical Tech. Lett.*, vol. 31, no. 6, pp. 411–415, Dec. 2001.

[99] M. T. Hill, H. J. S. Dorren, T. de Vries, X. J. M. Leijtens, J. H. den Besten, B. Smalbrugge, Y.-S. Oei, H. Binsma, G.-D. Khoe, and M. K. Smit, “A fast low-power optical memory based on coupled micro-ring lasers,” *Nature*, vol. 432, pp. 206–209, Nov. 2004.

ISBN 951-22-8304-2 (printed)

ISBN 951-22-8305-0 (PDF)

ISSN 1455-0474

Picaset Oy, Helsinki 2006